An integrative multi-omics approach to draft gene regulatory networks at a cell type resolution

Danila Voronov[1], Periklis Paganos[1], Marta S. Magri[2], Claudia Cuomo[1], Ignacio Maeso[2], Jose Luis Gómez-Skarmeta[2] and Maria Ina Arnone[1]*

[1]Stazione Zoologica Anton Dohrn, Villa Comunale, 80121, Naples, Italy
[2]Centro Andaluz de Biología del Desarrollo, CSIC/Universidad Pablo de Olavide, Sevilla, Spain

*Corresponding author: miarnone@szn.it

Abstract

Gene regulatory networks (GRNs) can be used to describe gene interactions of various complex biological processes such as embryonic development, regeneration and disease. The purple sea urchin *Strongylocentrotus purpuratus* endomesoderm developmental GRN has been a subject of multiple studies. Traditional approaches to drafting GRNs require embryological knowledge pertaining to the cell type families, information on the regulatory genes that control the regulatory state of the cell type family, causal data from gene knockdown experiments and validations of the identified interactions by cis-regulatory analysis, which helps identify the cis-regulatory modules (CRMs) of the regulatory genes. These approaches, while powerful, lacked information on whether the majority of these gene interactions are direct. The advent of a multitude of omics approaches involving next-generation sequencing (-seq) allows to obtain the necessary information for GRN drafting. Here we present a combinatorial omics method for *in silico* GRN drafting at high resolution, using i) a single cell RNA-seq derived cell atlas highlighting the 2 day post

fertilization (dpf) sea urchin gastrula cell type families, as well as the genes expressed at single cell level, ii) a set of putative CRMs and transcription factor (TF) binding sites obtained from chromatin accessibility ATAC-seq data, and iii) interactions directionality obtained from differential bulk RNA-seq following knockdown of the TF Sp-Pdx1, a key regulator of gut patterning in sea urchins. Using this method, we draft the GRN for the hindgut *Sp-Pdx1* positive cells in the 2 dpf gastrula embryo. Overall, our combinatorial approach highlights the complex connectivity of the posterior gut GRN as postulated in the past and increases the resolution and gene regulatory cascades operating within it.

Keywords

gene regulatory networks, sea urchin, embryo, gut, scRNA-seq, ATAC-seq, RNA-seq, Pdx1

Introduction

Gene regulatory networks (GRNs) are used to describe molecular underpinnings of developmental processes that lead to establishment of various cell and tissue types in a developing embryo. GRNs consist of two main components: genes, which are the nodes of the network, and their interactions, which are the edges of the network. Such networks allow visualization of inputs and outputs of transcription factors, signaling molecules and terminal differentiation genes in time and location specific manner.

Echinoderms and in particular the purple sea urchin *Strongylocentrotus purpuratus* has long been an experimental system for evolutionary developmental studies (Arnone et al., 2015; McClay, 2011). Together with hemichordates, echinoderms form the ambulacraria group, that is a phylogenetic sister group to chordates (Röttinger and Lowe, 2012). GRNs were used to study and describe the molecular underpinnings of the sea urchin embryonic development. The sea urchin endomesoderm GRN, in particular, is one of the best studied (Cary et al., 2020; Ettensohn, 2020; Peter and Davidson, 2010). In addition to that, the sea urchin embryonic gut GRN up until 3 days post fertilization (dpf) pluteus larva has also been a subject of multiple studies, reviewed in Annunziata et al. (2019), which showed the crucial role of Parahox genes, *Sp-Pdx1* and *Sp-Cdx,* in the development of the sea urchin hindgut and pyloric sphincter.

The traditional protocol for drafting GRNs requires embryological knowledge pertaining to the cell and tissue types present in the embryo, knowledge of the regulatory genes describing the regulatory state of the tissue or cell type, causal information from perturbation experiments and validations of the GRNs through the cis-regulatory analysis, identifying the cis-regulatory modules (CRMs) of the regulatory genes (Materna and Oliveri, 2008). The process of identification of the cell types and expressed genes usually involves gene expression visualization techniques such as *in situ* hybridization, while identification of CRMs is usually achieved via sequence alignment with evolutionary closely related species (Lee et al., 2007; Livi and Davidson, 2007) to identify conserved regions that could play a role as CRMs. Such methods allow identification of only a subset of the expressed

genes, usually highly expressed, for which *in situ* probes were made, and a limited number of CRMs around them. However, each cell expresses multiple genes that are controlled by various CRMs (Cui et al., 2017; de-Leon and Davidson, 2010; Paganos et al., 2021), thus high throughput approaches are essential to build full GRNs.

With the advent of novel technologies involving next generation sequencing, such as Assay for Transposase-Accessible Chromatin with next-generation sequencing (ATAC-seq) (Buenrostro et al., 2015), bulk and single cell RNA sequencing (RNA-seq and scRNA-seq, respectively) high throughput identification of CRMs and transcription factors (TFs) bound to them (2018), gene expression profiles (Davidson et al., 2022; Massri et al., 2021; Paganos et al., 2022c, 2021) and causal dynamics (Lowe et al., 2016; Rafiq et al., 2014) became possible. For example, Shashikant et al. (2018) used ATAC-seq to assess chromatin accessibility in sea urchin skeletogenic cells and were able to confirm previously known enhancers and identify more CRMs binding Sp-Alx1 and Sp-Ets1 TFs. Paganos et al. (2021) have used scRNA-seq data to identify the cell type families present in the 3 dpf pluteus of the sea urchin larvae and to get the expression profiles of genes within every identified cell population at unprecedented resolution.

Here we present a novel method of drafting GRNs for individual cells, cell types and tissues along with the cell type families atlas of the 2 dpf *S. purpuratus* gastrula obtained using single cell RNA-seq data and the set of putative gut CRMs at 2 dpf obtained with embryonic gut and whole embryo ATAC-seq. The method, while following the established logic for drafting GRNs (Materna and Oliveri, 2008), provides insight to whether the GRN interactions are direct or not while at the same time increasing the resolution of the existing GRN. In this study, we use ATAC-seq data for predicting CRMs and performing TF footprinting along with scRNA-seq data to narrow genome wide predictions to specific cell type families. Furthermore, we use the available bulk differential RNA-seq data to give causal information to the interactions within a GRN of the cells of the hindgut expressing the key gut patterning ParaHox gene *Sp-Pdx1* (Annunziata and Arnone, 2014; Cole et al., 2009). Additionally, we present an overview of the GRN of the sea urchin 2 dpf gastrula stage hindgut obtained with this method.

Results

Gastrula stage embryo and gut chromatin accessibility assessment

In order to identify the locations of putative CRMs (pCRMs) in the sea urchin gastrula and predict which TFs are bound to them, we have generated ATAC-seq libraries for the sea urchin gastrula whole embryo and the gut tissue in two replicates each. The list of concordant peaks was obtained by merging all the independent peaks from gut and whole embryo ATAC-seq data resulting in 30866 open chromatin regions (OCRs) (Supplementary file 1). Majority of those OCRs are in the intergenic regions (40.44%) and in the introns (28.27%), promoter regions have 12.95% of the open chromatin peakset (Figure 1A). We have also performed TF footprinting analysis to find which TFs could be bound at those OCRs. This resulted in 279197 footprints genome-wide (Supplementary file 2), with 36.06% of them in the intergenic OCRs, 27.10% in the intronic OCRs and 17.10% in the promoter-TSS associated OCRs (Figure 1B). In order to assess whether the OCRs correspond to pCRMs, we have looked for the presence of published confirmed cis regulatory regions in our concordant peakset. To do this, we have looked for overlap between the confirmed published hindgut CRMs (Arnone et al., 1998; Cui et al., 2017; de-Leon and Davidson, 2010; Lee et al., 2007; Livi and Davidson, 2007; McCarty and Coffman, 2013; Smith et al., 2008) and our 2 dpf stage concordant peaks. We have found that out of 22 confirmed published CRMs, 18 are present in the concordant peak set (Figure 1C). For instance, our data recovers all the three known CRMs for *Sp-Blimp1*: regions CR3, CR5 and 43 (Smith et al., 2008) (Figure 1D). Our data also improves resolution of CRM prediction since the open chromatin and thus active region of CRM E of *Sp-Hox11/13b* is confined to a 503 bp long peak inside of 4988 bp of the identified CRM E (Cui et al., 2017). This indicates that the concordant peakset represents pCRMs for the 2 dpf stage embryos. Some of the known CRMs were not found, such as CRM D for *Sp-Hox11/13b (Cui et al., 2017)* (Figure 1D), which could most likely be due to these locations being open at different stages of development and, therefore, were not further analyzed in this study. Our dataset also allowed us to identify novel CRMs as exemplified by pCRMs around the key posterior gut patterning drivers *Sp-Pdx1* and *Sp-Cdx* (Annunziata and Arnone, 2014;

Cole et al., 2009). Specifically, there are five putative CRMs for *Sp-Pdx1* and four for *Sp-Cdx* at 2 dpf (Figure 1E). *Sp-Pdx1* CRMs will be further explored in later sections of this manuscript.

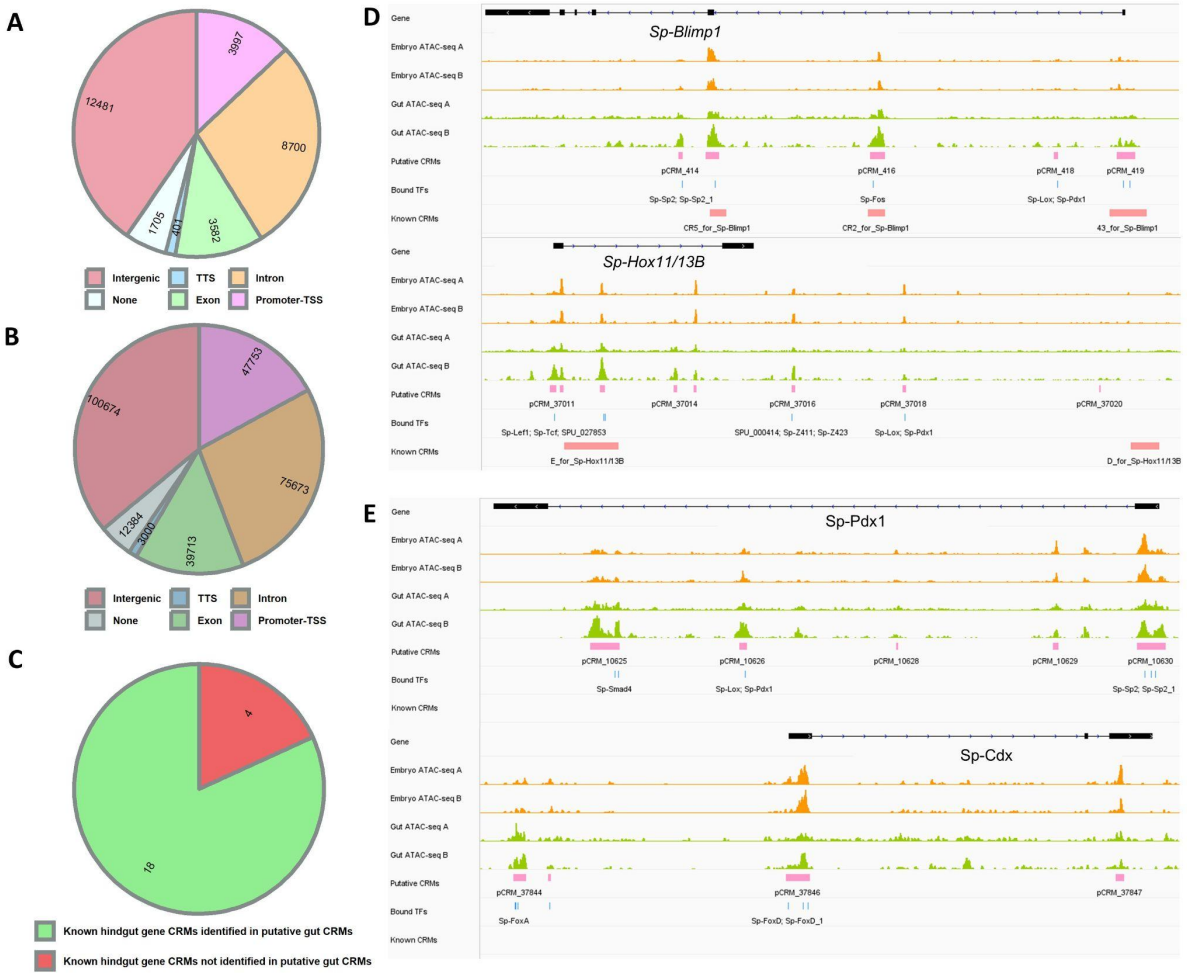

Figure 1. Open chromatin regions in the sea urchin gastrula. A) Pie chart of the proportion of putative CRMs relative to the genome annotation features. **B)** Pie chart of the proportion of transcription factor footprints in pCRMs associated with genome annotation features. **C)** Pie chart of the proportion of presence of published known hindgut CRMs in the ATAC-seq predicted putative CRMs at 2 dpf. **D)** Genome browser tracks of *Sp-Blimp1* and *Sp-Hox11/13b* putative CRMs overlapping with published CRMs for those genes. **E)** Genome browser tracks of *Sp-Pdx1* and *Sp-Cdx* putative CRMs. No CRMs were previously published for these genes

Diversity of cell type families in the sea urchin gastrula

In order to identify cell type specific GRNs in the 2 dpf *S. purpuratus* late gastrula stage we performed scRNA-seq on five samples originating from three independent biological replicates. Embryos were dissociated into single cells using an

enzyme-free dissociation protocol, previously developed in our group (Paganos et al., 2021), which allows the sequencing of alive and healthy cells. Isolated single cells were processed using the 10x Chromium scRNA-seq capturing system (Figure 2A). In total, transcriptomes from 15,341 cells were included in the final analysis. Computational analysis, including data integration and Louvain graph clustering resulted in the identification of 20 distinct cell clusters (Figures 2A and 2E), corresponding to individual cell types or a set of closely related cell types.

Next, we undertook the task to explore the identity of the 20 identified cell clusters. Cell type family identities were assigned to each cluster based on the expression of previously described cell type markers, exploration of the total amount of genes expressed within them (Supplementary file 3), as well as taking advantage of the transcriptional signatures previously identified in the 3 dpf pluteus larva through scRNA-seq (Paganos et al., 2021) (Figure 2B, Figure 2—figure supplement 1). For instance, the following genes were used as specific cell type markers allowing us to recognize distinct cell type families: ciliary band (*Sp-Hnf6, Sp-Fbsl_2*) (Paganos et al., 2021; Poustka et al., 2004), anterior neuroectoderm (*Sp-Frizz5/8*) (Cui et al., 2014), aboral ectoderm (Spec1, SPU_006199) (Amore et al., 2003; Paganos et al., 2021), oral ectoderm (*Sp-Bra* and *Sp-FoxABL*) (Paganos et al., 2021; Wei et al., 2012), neurons (*Sp-Synb*) (Burke et al., 2006), myoblasts (*Sp-FoxC, Sp-Mlckb*) (Andrikou et al., 2013; Paganos et al., 2021), small micromere descendants (*Sp-Nan2* and *Sp-Vasa*) (Juliano et al., 2010), globular cells (*Sp-MacpfA2*) (Ho et al., 2017), immune cells (*Sp-Pks1, Sp-Hypp_1249)* (Paganos et al., 2021; Perillo et al., 2020), blastocoelar cells (*Sp-Fcoll/II/III*) (Paganos et al., 2021), skeleton (*Sp-Msp130, Sp-Hypp_2386*) (Harkey et al., 1992; Paganos et al., 2021), hindgut (*Sp-Hox11/13b*, *Sp-Cdx*, *Sp-FoxI*) (Annunziata and Arnone, 2014; Tu et al., 2006), midgut (*Sp-Chp*, *Sp-ManrC1a*) (Annunziata et al., 2019; Annunziata and Arnone, 2014), exocrine pancreas-like precursors (*Sp-Ptf1a*) (Paganos et al., 2022b; Perillo et al., 2016) and foregut (*Sp-Brn1/2/4*) (Cole and Arnone, 2009). As the ultimate goal of this study is the reconstruction of the posterior gut GRN and especially the one that is orchestrated by the TF Sp-Pdx1, we further explored our data by plotting for *Sp-Pdx1* as well as TFs known to pattern distinct domains of the posterior archenteron (Annunziata and Arnone, 2014; Paganos et al., 2021) (Figure 2C). Our analysis revealed that the majority of these TFs are expressed in the two clusters

that we recognized as hindgut, supporting our cell type annotation. Interestingly, transcripts for *Sp-Pdx1* and, in total, eleven out of the thirteen investigated TFs were found present in the Hindgut (1) cluster. In more detail, the molecular fingerprint of this cell type family as revealed by scRNA-seq, includes the TFs Sp-FoxA, Sp-SoxC, Sp-Blimp1, Sp-Gatae, Sp-Pdx1, Sp-Rhox3, Sp-FoxI, Sp-Cdx, Sp-Bra and Sp-Hox11/13b. Furthermore, the presence of the TFs Sp-Bra and Sp-Hox11/13b in this cluster, known to be expressed in the most posterior part of the developing archenteron, confirms that this cell type family corresponds to the most posterior hindgut domain, even though *Sp-Pdx1* and *Sp-Bra* are not expressed in the same cells of this domain as revealed by FISH (Figure 2- figure supplement 2). This suggests heterogeneity of the Hindgut (1) cluster containing cells corresponding to more than one cell type.

Finally, to confirm the identities assigned to the cell clusters, we performed *in situ* hybridization on a selected set of genes with known and unknown expression patterns at this stage (Figure 2D). The FISH results were in line with the initial predictions and our cell type annotation. Similar to our previous findings in the case of the 3 dpf *S. purpuratus* pluteus larva (Paganos et al., 2021), there is one cluster with poorly defined molecular signature that likely represents not fully differentiated cells, which we refer to as undefined. The persistence of this cluster at both timepoints is indicative of this cluster representing an actual cell type rather than it being a technical artifact.

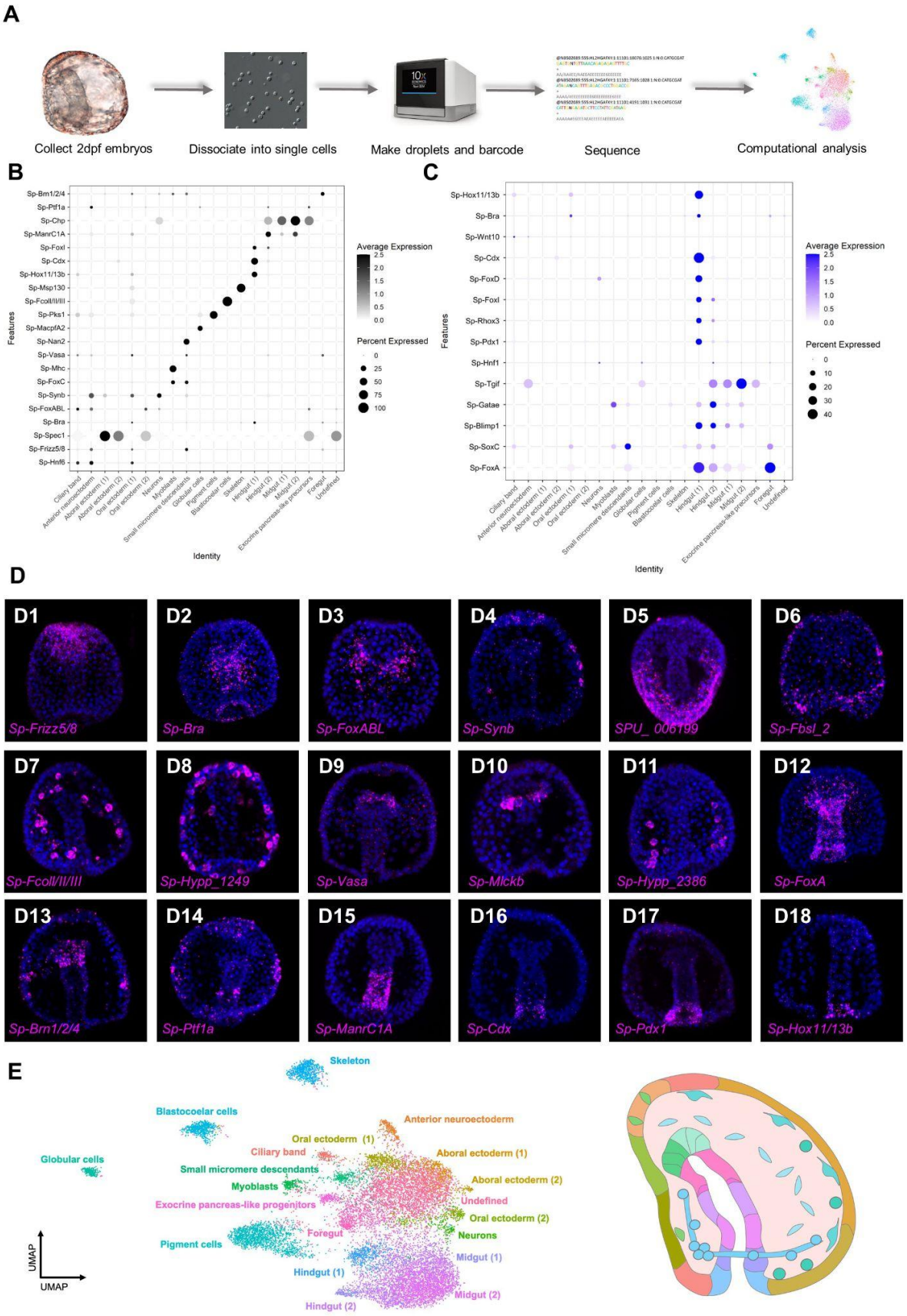

Figure 2. Cell type family atlas of the 2 dpf *S. purpuratus* gastrula stage. **A)** General scheme of scRNA-seq data generation and analysis. **B)** Dotplot of marker genes used for

determining cluster identities. **C)** Dotplot of known hindgut genes, highlighting expression in the Hindgut (1) cluster. **D)** FISH of *S. purpuratus* 2 dpf gastrula embryos using antisense probes for *Sp-Frizz5/8* (D1), *Sp-Bra* (D2), *Sp-FoxABL* (D3), *Sp-Synb* (D4), *SPU_006199* (D5), *Sp-FcoI/II/III* (D6), *Sp-Hypp_1249* (D7), *Sp-Vasa* (D9), *Sp-Mlckb* (D10), *Sp-Hypp_2386* (D11), *Sp-FoxA* (D12), *Sp-Brn1/2/4* (D13), *Sp-Ptf1a* (D14), *Sp-ManrC1A* (D15), *Sp-Cdx* (D16), *Sp-Pdx1* (D17), *Sp-Hox11/13b* (D18). All embryos are oriented in oral view, except embryos shown in panels D7 and D14 that are oriented in lateral view and D5 that is placed in dorsal view. Nuclei are depicted in blue (DAPI). **E)** Uniform Manifold Approximation and Projection (UMAP) plot of identified cell clusters in 2 dpf gastrula, with the clusters highlighted in a schematic representation of 2 dpf sea urchin gastrula using color-coding.

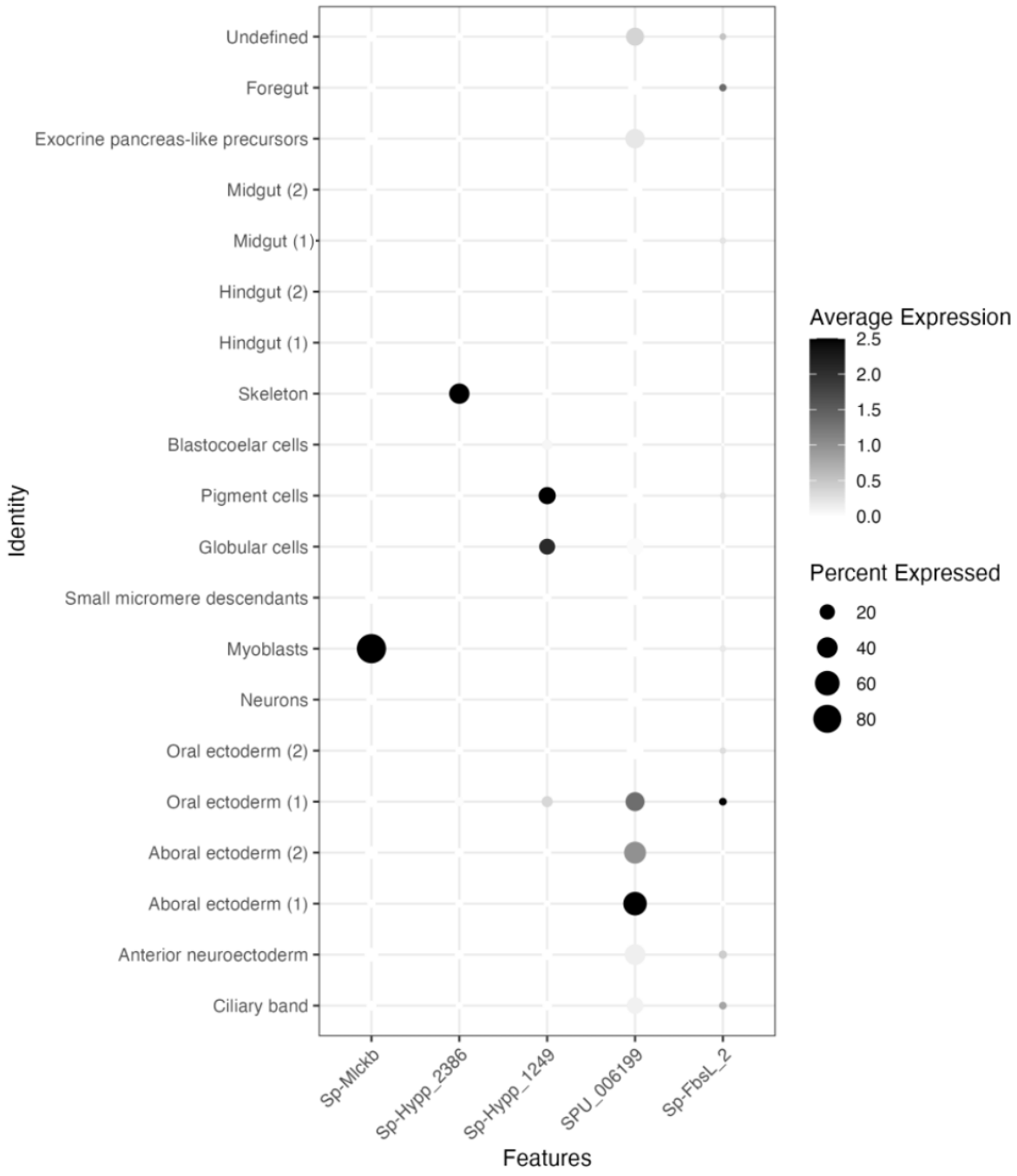

Figure 2- figure supplement 1. Dotplot of additional marker genes used for determining cluster identities.

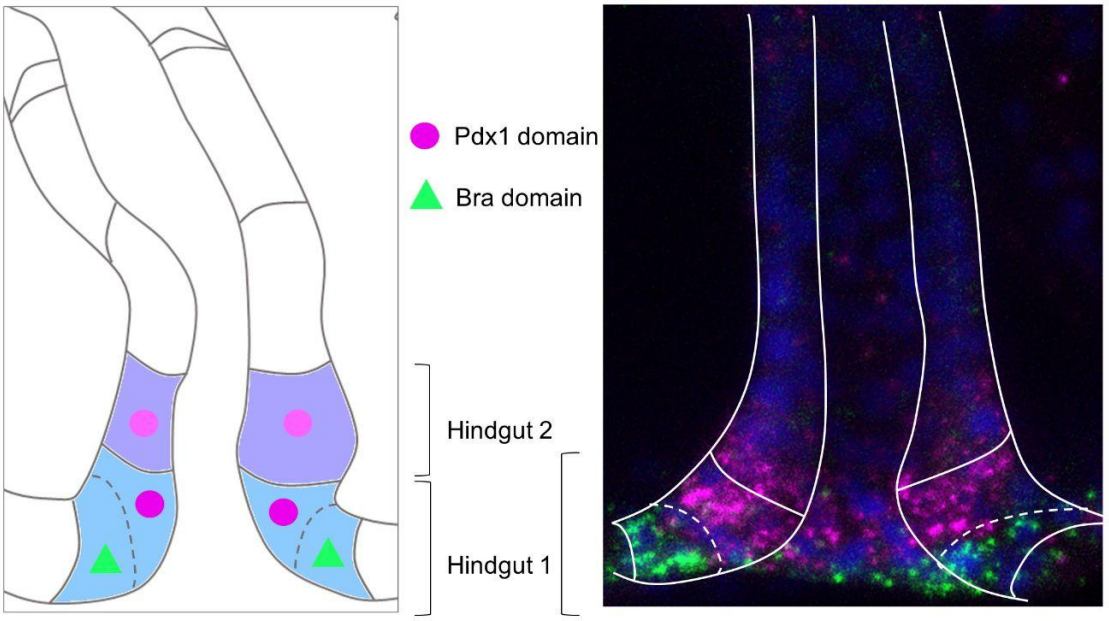

Figure 2- figure supplement 2. Schematic representation (left panel) and double FISH (right panel) showing *Sp-Pdx1* and *Sp-Bra* expression in different cells of the Hindgut (1) cluster.

RNA-seq data uncovers the targets of Sp-Pdx1 in the developing gut

Causal information about the function of a gene is crucial to drafting GRNs. Taking advantage of the already available bulk RNA-seq data after Pdx1 knockdown at 2 dpf gastrula obtained from Annunziata and Arnone (2014), after re-analysis using up-to-date differential expression analysis pipeline, we were able to get the list of differentially expressed genes (DEGs) between the untreated sea urchin embryos and those that were injected with *Sp-Pdx1* morpholino oligonucleotide (MO) (Cole et al., 2009). Moreover, this allowed us to provide additional information regarding these libraries. The principle component analysis (PCA) performed on the untreated and injected groups of embryos showed that 97% of variance between the samples is explained by the injection of the *Sp-Pdx1* morpholino (Figure 3A), which indicates that the difference in gene expression is due to the *Sp-Pdx1* perturbation and, thus, the dataset can be used to infer causal information downstream of Sp-Pdx1. In line with previous findings, our differential expression analysis identified a large number of deregulated genes totaling to 2680 DEGs with adjusted *p*-value of less than 0.05

(Supplementary file 4). Of those, 1661 were upregulated after *Sp-Pdx1* perturbation and 1019 were downregulated (Figure 3B). According to scRNA-seq *Sp-Pdx1* positive cells are found in the hindgut (clusters Hindgut (1) and Hindgut (2)),, in the midgut (clusters Midgut (1) and Midgut (2)) as well as a low number of cells in the clusters corresponding to oral ectoderm (oral ectoderm cells (2)) and ciliary band (Figure 3D). Notably, average scaled expression of this gene in clusters other than Hindgut (1) is less than 0.5 (Figure 2C, Supplementary file 3). Using the bulk and scRNA-seq data the cell families of differentially expressed genes could be inferred (Figure 3C). The downregulated genes, thus those that are activated by Sp-Pdx1 in the untreated embryos, belong to gut cell families, especially to the hindgut cell clusters, while the upregulated genes belong mostly to the anterior neuroectoderm and ciliary band cell clusters, although there are some genes in the anterior neuroectoderm that are downregulated after Sp-Pdx1 MO (Figure 3C and E). Consequently, the RNA-seq data sheds light on what genes are downstream of Sp-Pdx1 and whether they are up or downregulated by this TF.

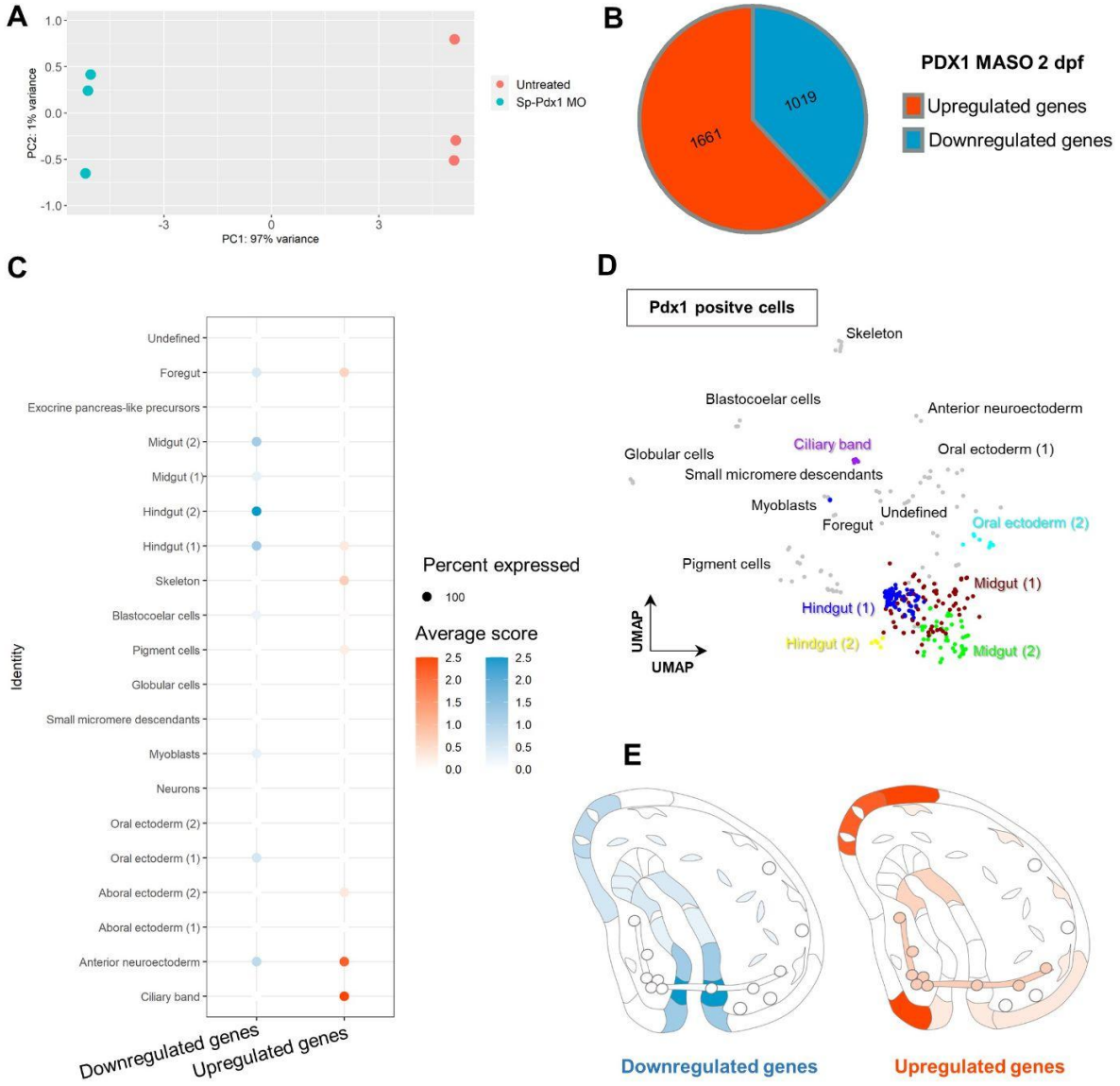

Figure 3. Differential RNA-seq of Sp-Pdx1 knockdown embryos. A) Principal component analysis (PCA) plot highlighting the variance explained by the morpholino treatment. **B)** Pie chart of proportion of significant genes up- and down-regulated after Sp-Pdx1 knockdown. **C)** Dotplot of cell clusters to which up- and down-regulated genes belong. **D)** UMAP plot of cells within the identified cell clusters at 2 dpf that express *Sp-Pdx1*. **E)** Diagrams of sea urchin 2 dpf gastrula highlighting the localization of up- and down-regulated genes.

Pipeline for *in silico* GRN drafting

The combination of the data described in all the aforementioned sections has enabled us to draft GRNs at an unprecedented resolution and unravel the potential gene regulatory interactions controlling sea urchin posterior gut development. The

general flowchart of the method is described in Figure 4. The ATAC-seq dataset can be used to predict two important components that allow describing the nodes and interactions within a GRN: putative CRMs obtained from concordant peakset and TFs bound to these putative CRMs obtained from the ATAC-seq footprinting analysis. Single cell data allows narrowing these genome wide and gut tissue wide predictions to a specific cell type family or to a cell population within a cell type family expressing a gene of interest. Therefore, we applied this method for Sp-Pdx1 expressing cells in the Hindgut (1) cell cluster of the 2 dpf *S. purpuratus* embryo. ScRNA-seq data shows which of the TFs, predicted using solely ATAC-seq data, are actually expressed in the cell population of interest. Differential RNA-seq data helps obtain causal information on interactions of nodes of the hindgut GRN downstream of Sp-Pdx1 by analyzing which genes are affected by its perturbation and how. ATAC-seq data allows to show which of the interactions are direct, while combination of ATAC-seq and RNA-seq also allows to find the most parsimonious way of explaining interactions between various levels of indirect Sp-Pdx1 targets through iterative assignment of interaction signs. For instance, the *Sp-Pdx1* gene in this case is the effector gene (Efct) that has direct (D-tgt) and indirect (I-tgt) targets (Figure 4- figure supplement 1). For instance, if a direct target of Sp-Pdx1 (D-tgt1) is expressed less when Sp-Pdx1 is knocked down and its direct target, thus indirect Sp-Pdx1 target (I-tgt1) is also expressed less when Sp-Pdx1 is knocked down, then Sp-Pdx1 TF activates the D-tgt1 and D-tgt1 in turn activates I-tgt1 (Figure 4- figure supplement 1). While, if an indirect Sp-Pdx1 target (I-tgt2), which is a direct target of a direct Sp-Pdx1 target, is downregulated by Sp-Pdx1 MO, thus upregulated by Sp-Pdx1 TF, and the direct Sp-Pdx1 target (D-tgt2) is downregulated by Sp-Pdx1 TF, then we can deduce that D-tgt2 downregulates the I-tgt2 (Figure 4- figure supplement 1). Same approach can be used with the combination of up-regulating and down-regulating interactions, such as activation of I-tgt3 by Sp-Pdx1 (Figure 4- figure supplement 1). This process can be performed iteratively for other indirect targets that have more intermediates between them and *Sp-Pdx1* to assign signs to interactions downstream of Sp-Pdx1. The IDs used throughout the pipeline are then converted to gene names for visualization in BioTapestry software. This method allows to draft detailed GRNs with direct and indirect interactions per cell type family, highlighting the depth of the GRN.

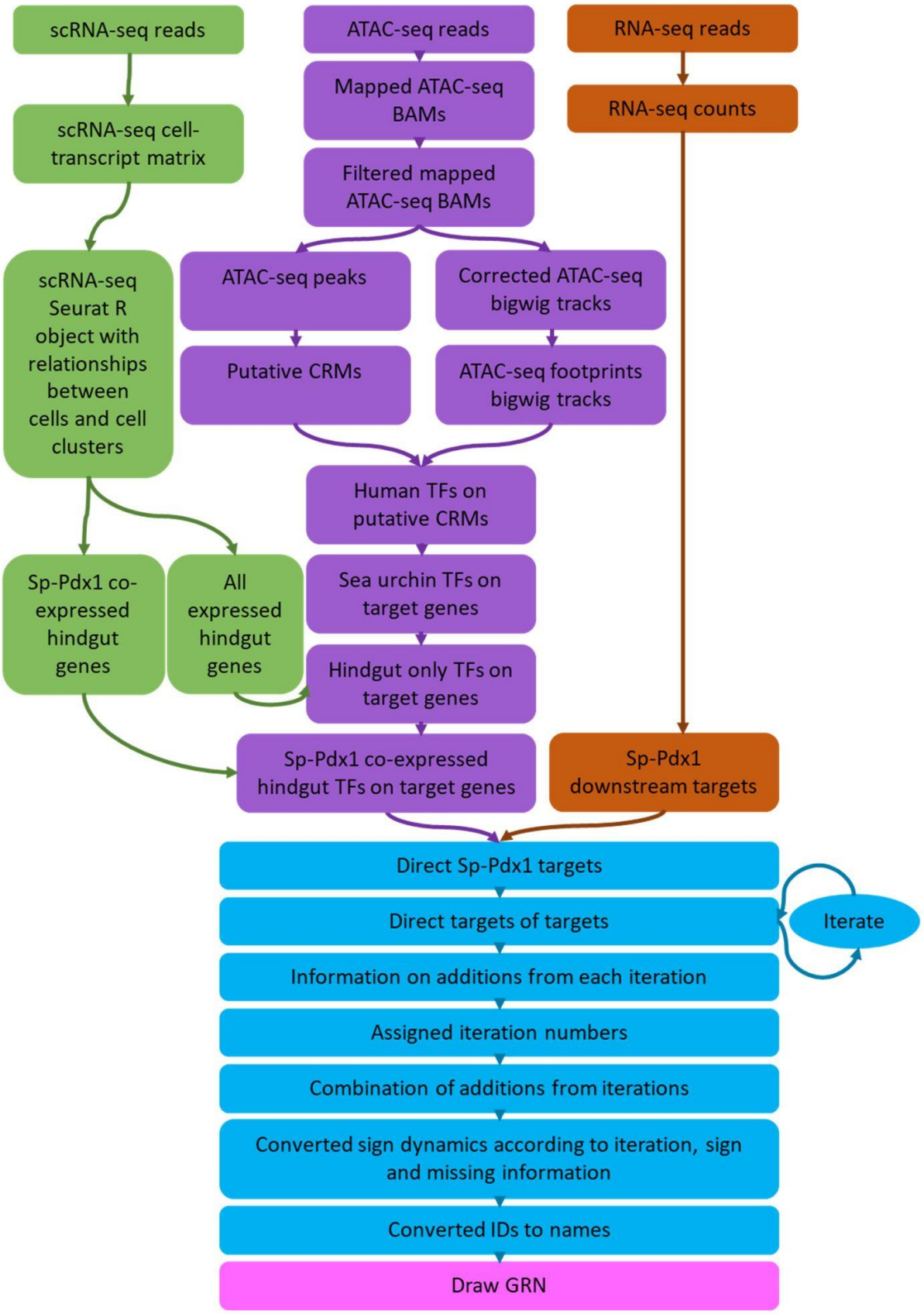

Figure 4. Flowchart of the *in silico* GRN drafting pipeline. Colors represent analysis performed on different data types. Analysis of scRNA-seq data is green, analysis of

ATAC-seq data is purple, analysis of differential RNA-seq following Sp-Pdx1 knockdown is brown, combination of the datasets and downstream analysis is blue, drawing the GRN is pink.

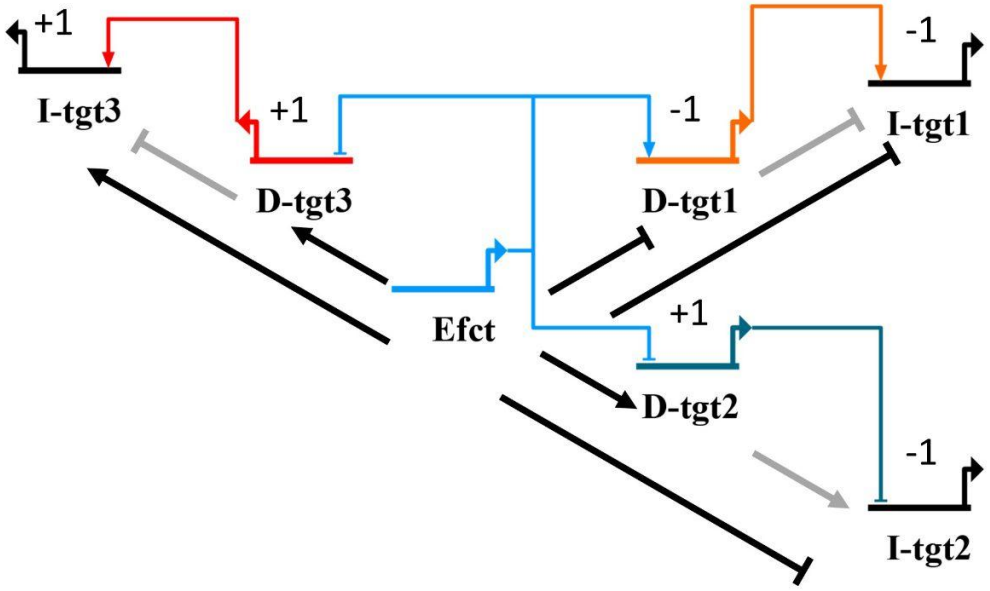

Effector gene (Efct), knock down of which resulted in differential RNA-seq data, has direct (D-tgt) and indirect (I-tgt) targets. The differential RNA-seq data shows whether after knock down of Efct target genes, both direct and indirect, increase in expression or decrease, as indicated by +1 and -1 respectively. Same is also shown by black pointed and blunt arrows, as it shows the overall effect of gene expression of Efct knockdown. The missing information on interactions between D-tgts and respective I-tgts (grey arrows) can be obtained using the known overall effect of Efct on all its direct and indirect targets from the differential gene expression analysis. This allows to obtain the most parsimonious interactions between Efct, D-tgts and I-tgts (colored GRN interactions).

Figure 4- figure supplement 1. Schematic representation of sign assignment logic used for GRN drafting.

Gastrula hindgut Gene Regulatory Network

Using our pipeline it is possible to draft GRNs for any individual cell type, tissue or organ. For instance the complete GRN for the 2 dpf gastrula hindgut can be drafted,

in particular, the interactions between various TFs involved in building the embryonic hindgut with 512 interactions involving 91 individual TFs (Figure 5- figure supplement 1A, Supplementary file 5). This GRN can be narrowed down keeping only the nodes that are co-expressed with *Sp-Pdx1* in the same cells (Figure 5- figure supplement 1B, Supplementary file 6). Previously, the core of the hindgut GRN was reconstructed by Annunziata and Arnone (2014) and a global genome view of the GRN operating within the nuclei of these cells was reviewed in Annunziata et al. (2019). Our combinatorial omics approach allows us to update and refine the published GRN for the hindgut region and reconstructing the one for Sp-Pdx1 positive cells at higher resolution.

The GRN presented in Annunziata et al. (2019) (Figure 5A), which represents the most complete version of the posterior gut at that time, shows possible interactions between the different genes comprising it. However, with the available data at that point it was unclear whether these interactions could be direct or indirect. Using our pipeline towards answering the very same question, we found that most of them appear to be indirect and each gene is wired through one or more intermediate nodes. Bellow we report several cases for which we present a refined and/or alternative gene regulatory connectivity:

Sp-Pdx1

Sp-Pdx1 was shown to control Sp-Cdx (Figure 5A), however the actual link between the two remained an open question. Our data suggests that this interaction is likely indirect since there are no Sp-Pdx1 TF binding sites above the threshold near *Sp-Cdx*. This interaction may instead be routed through either Sp-FoxD or Sp-Osr (Figure 5B) as revealed by this study.

Sp-Hox11/13b

Sp-Hox11/13b was previously shown to have a self repressive loop and an input on *Sp-Cdx* (Figure 5A). The combinatorial data, again, favors the indirect nature of the self control loop. This loop can instead be wired through Sp-Pdx1, which represses *Sp-Hox11/13b* expression. Additionally, the effect Sp-Hox11/13b on *Sp-Cdx* can be explained through Sp-Hox11/13b direct activation of *Sp-Osr*, which then in turn

affects *Sp-Cdx* directly. We also identify a direct input of Sp-Hox11/13b on *Sp-Pdx1*, which was not reported before (Figure 5C).

Sp-Cdx

Similarly to *Sp-Hox11/13b*, *Sp-Cdx* also has a self regulatory loop (Figure 5A). In this case our combinatorial approach also suggests multiple equivalent indirect paths from Sp-Cdx back to *Sp-Cdx* that is in line with the *Sp-Cdx* self regulation previously reported, such as through Sp-Runt1 to Sp-Blimp1 onto *Sp-FoxD* and then to *Sp-Cdx* (Figure 5D).

Sp-Gatae

Sp-Gatae was shown to have an activatory effect on *Sp-Hox11/13b* and on itself (Figure 5A). Our data indicates that these effects are also indirect, and that the path to *Sp-Hox11/13b* can go through upregulating *Sp-Blimp1*, which itself upregulates *Sp-Hox11/13b*. The effect on *Sp-Hox11/13b* can also be explained through the same intermediates that are likely to account for the self feedback loop of Sp-Gatae such as Sp-Irf and Sp-SoxC (Figure 5E).

Sp-Blimp1

Sp-Blimp1 was previously shown to affect *Sp-Pdx1* (Figure 5A), and it is likely that this interaction occurs through a single intermediate, either Sp-Tcf or Sp-Hox11/13b or possibly both. Thus, this interaction between Sp-Blimp1 and *Sp-Pdx1* is also not direct (Figure 5F).

Sp-FoxA

In the published GRN, *Sp-FoxA* has many outputs: Sp-FoxA, Sp-Cdx, Sp-Hox11/13b and Sp-Bra (Figure 5A). The input on *Sp-Cdx* could be a direct one, as supported by TF *in silico* footprinting. The data for the rest of the interactions suggests that they are indirect and happen through intermediates. Sp-FoxA is likely to affect itself through a loop via Sp-Hb9, while the input on *Sp-Hox11/13b* can be explained via Sp-Osr or Sp-Runt1 to Sp-Tcf activations. Sp-Tcf, eventually, has a direct input on *Sp-Hox11/13b* (Figure 5G).

Sp-Bra

Sp-Bra is not expressed in the hindgut cells expressing *Sp-Pdx1* at the 2 dpf gastrula stage (Figure 2- figure supplement 2), but going back to include all the cells of the hindgut (1) cluster its wiring can also be recovered (Figure 5- figure supplement 2). Our data confirms the direct input of Sp-Bra on *Sp-FoxA* with an Sp-Bra footprint proximally to the *Sp-FoxA* gene (de-Leon and Davidson, 2010; Schwaiger et al., 2022), while the Sp-Bra effect on *Sp-Cdx* is likely indirect and could go either through Sp-FoxA or Sp-Osr as intermediates. In addition, our data at 2 dpf suggest that the inputs of Sp-FoxA on *Sp-Bra* and on itself are indirect, the effect on *Sp-Bra* could be wired through Sp-Tcf and Sp-Cdx, Sp-Runt1 and Sp-Osr intermediates, while self-feedback loop of Sp-FoxA is to be explained by a loop through Sp-Tcf and Sp-Bra (Figure 5- figure supplement 2).

All together, our approach not only allows correct reconstruction of a GRN without prior knowledge, but also empowers better resolution of the interactions identified previously by supplementing additional information on whether these interactions are direct or indirect and by identifying the intermediate nodes within cells of interest through combinatorial omics.

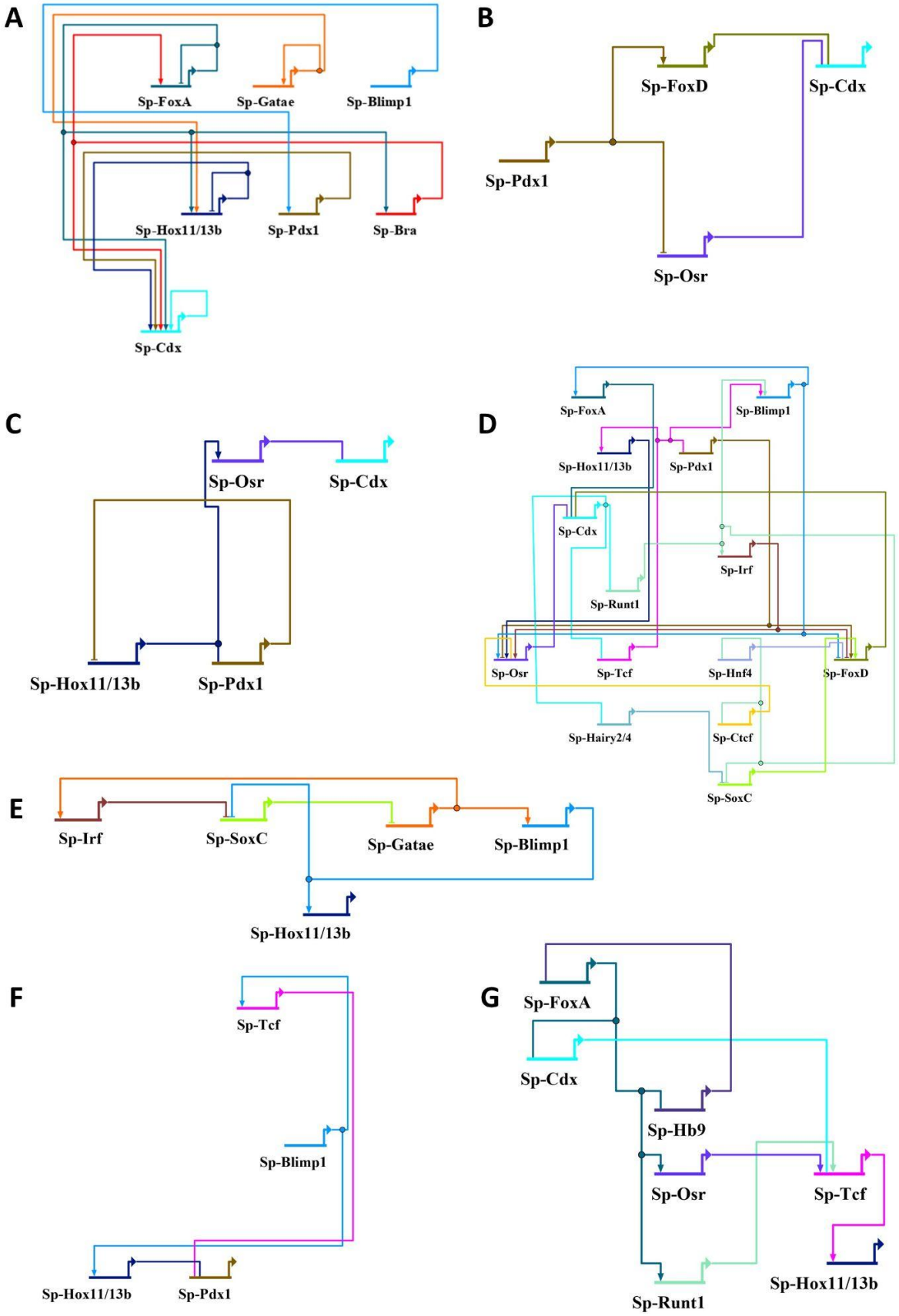
A
Sp-FoxA
Sp-Gatae
Sp-Blimp1
Sp-Hox11/13b
Sp-Pdx1
Sp-Bra
Sp-Cdx
B
Sp-FoxD
Sp-Cdx
Sp-Pdx1
Sp-Osr
C
Sp-Osr
Sp-Cdx
Sp-Hox11/13b
Sp-Pdx1
D
Sp-FoxA
Sp-Blimp1
Sp-Hox11/13b
Sp-Pdx1
Sp-Cdx
Sp-Irf
Sp-Runt1
Sp-Osr
Sp-Tcf
Sp-Hnf4
Sp-FoxD
Sp-Hairy2/4
Sp-Ctcf
Sp-SoxC
E
Sp-Irf
Sp-SoxC
Sp-Gatae
Sp-Blimp1
Sp-Hox11/13b
F
Sp-Tcf
Sp-Blimp1
Sp-Hox11/13b
Sp-Pdx1
G
Sp-FoxA
Sp-Cdx
Sp-Hb9
Sp-Osr
Sp-Tcf
Sp-Hox11/13b
Sp-Runt1

Figure 5. 2 dpf *S. purpuratus* gastrula stage hindgut gene regulatory networks. **A)** Global genome view of the core TFs operating in the 2 dpf hindgut GRN as reviewed in Annunziata et al. 2019. **B)** *In silico* drafted GRN connecting Sp-Pdx1 with downstream genes of the core GRN. **C)** *In silico* drafted GRN connecting Sp-Hox11/13B with downstream genes of the core GRN. **D)** *In silico* drafted GRN connecting Sp-Cdx with downstream genes of the core GRN. **E)** *In silico* drafted GRN connecting Sp-Gatae with downstream genes of the core GRN. **F)** *In silico* drafted GRN connecting Sp-Blimp1 with downstream genes of the core GRN. **G)** *In silico* drafted GRN connecting Sp-FoxA with downstream genes of the core GRN.

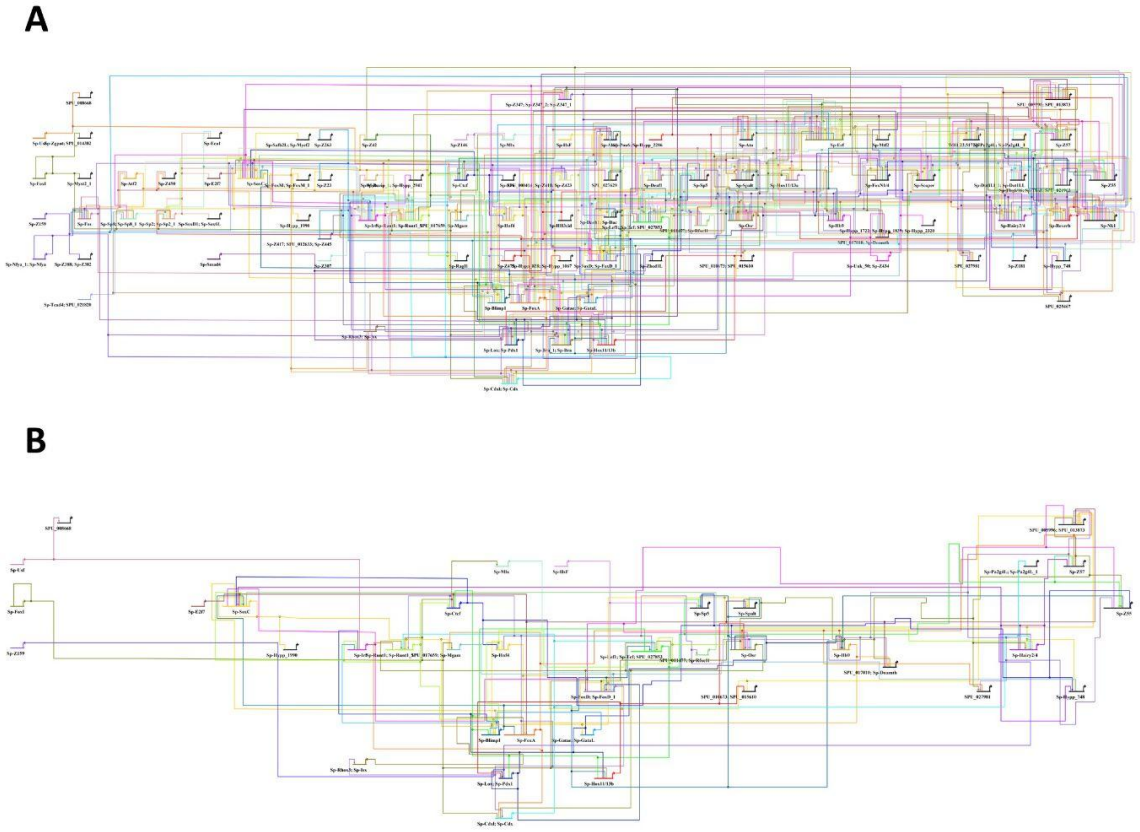

Figure 5- figure supplement 1. 2 dpf *S. purpuratus* gastrula stage hindgut gene regulatory networks. **A)** Full gene regulatory network of the transcription factors of the 2 dpf sea urchin gastrula hindgut (1) cluster. **B)** Full gene regulatory network of the transcription factors of the Sp-Pdx1 positive cells within the hindgut (1) cluster.

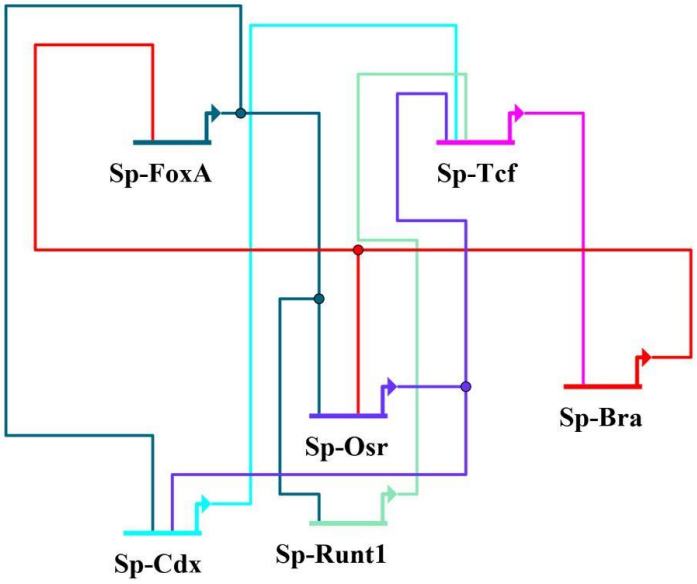

Figure 5- figure supplement 2. Gene regulatory network connecting Sp-FoxA and Sp-Bra within the published GRN highlighting the indirect nature of this interaction.

CRM5 allows control of *Sp-Pdx1* by Sp-Hox11/13b

The identified direct input of Sp-Hox11/13b on *Sp-Pdx1* was not reported previously and, therefore, is of great interest. Consequently, we focused our attention on exploring this input. Our CRM predictions and the TF footprinting indicates a binding site for Sp-Hox11/13b in the pCRM5 which is in the 5' of the gene and overlaps the first exon of the *Sp-Pdx1* gene (Figure 6A). To determine whether this pCRM is indeed an active cis-regulatory element, a GFP reporter construct with this element was microinjected into *S. purpuratus* zygotes. The microinjected embryos were allowed to develop until 2 dpf gastrula stage and then GFP expression driven by this pCRM was visualized. At 2 dpf, the CRM5-GFP-tag construct exhibits expression consistent with the known Pdx1 positive domains including the lateral neurons, (Figure 6B and G) and the hindgut regions (Figure 6C and G) as well as other regions of the gut such as the future stomach (Figure 6D and G). At 3 dpf pluteus stage, this CRM is capable of driving GFP expression in the predominant Pdx1 expression domain in the larval digestive tract, specifically, in the pyloric sphincter (Figure 6E). To determine whether Sp-Hox11/13b could affect *Sp-Pdx1* expression through CRM5, Sp-Hox11/13b morpholino oligonucleotide (Arenas-Mena et al., 2006) was co-injected with the CRM5 GFP reporter construct. At 2 dpf, the presence

of the Sp-Hox11/13b morpholino decreases the overall reporter construct expression, in addition to greatly inhibiting the GFP expression in the endodermal regions, such as the hindgut (Figure 6F and G), with more than ten-fold decrease in the percentage of endodermally expressing embryos (Figure 6G). This indicates that Sp-Hox11/13b could control *Sp-Pdx1* expression in the hindgut through *Sp-Pdx1* CRM5.

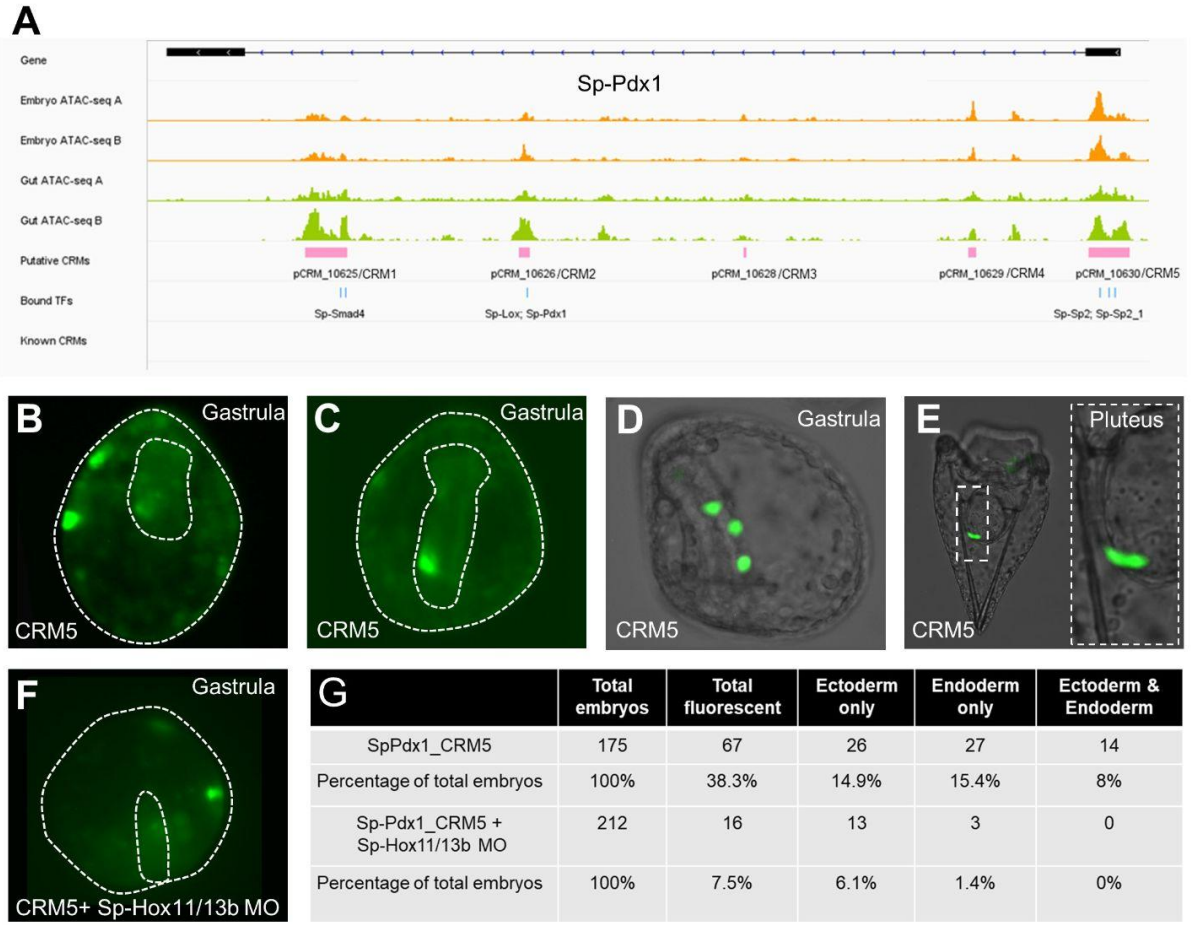

G	Total embryos	Total fluorescent	Ectoderm only	Endoderm only	Ectoderm & Endoderm
SpPdx1_CRM5	175	67	26	27	14
Percentage of total embryos	100%	38.3%	14.9%	15.4%	8%
Sp-Pdx1_CRM5 + Sp-Hox11/13b MO	212	16	13	3	0
Percentage of total embryos	100%	7.5%	6.1%	1.4%	0%

Figure 6. Sp-Pdx1 CRM5 control of *Sp-Pdx1*. A) Genome browser tracks of *Sp-Pdx1* putative CRMs. **B)** Sp-Pdx1 CRM5 driven GFP expression in the lateral neurons of the 2 dpf gastrula stage. C) Sp-Pdx1 CRM5 driven GFP expression in the hindgut of the 2 dpf gastrula stage. D) Sp-Pdx1 CRM5 driven GFP expression in the midgut of the 2 dpf gastrula stage. **E)** Sp-Pdx1 CRM5 driven GFP expression in the midgut of the 3 dpf pluteus. **F)** Sp-Pdx1 CRM5 driven GFP expression in the 2 dpf gastrula stage indicating absence of endodermal expression after Sp-Hox11/13b knockdown. **G)** Embryo scoring table showing the effect of Sp-Hox11/13b knockdown on the Sp-Pdx1 CRM5 driven GFP expression in different germ layers.

Multi-omics increases hindgut GRN resolution

Combinatorial omics and in vivo validations allow drafting an updated version of the GRN published in Annunziata and Arnone (2014) within the cells that express the Sp-Pdx1 transcription factor (Figure 7). Chromatin accessibility information allowed us to identify putative CRMs and TF binding sites within them, while single cell data allowed us to filter those to contain only genes from cells that express the *Sp-Pdx1* gene. Such filtering to cells expressing a particular TF allows us to assess its role controlling downstream genes in the same cells, when adding the bulk RNA-seq data after *Sp-Pdx1* knockdown. This gives a highly detailed and novel GRN for a particular subset of hindgut cells expressing *Sp-Pdx1* cells. Notably, these cells express all the TFs present in the GRN reviewed in Annunziata et al. (2019) except *Sp-Bra*. The reasoning for this is that at 2 dpf *Sp-Bra* is expressed in a different subset of Hindgut (1) cells and is not co-expressed with *Sp-Pdx1*, thus it was excluded from the updated GRN (Figure 7, Figure 2- figure supplement 2). *Sp-Hox11/13b* MO injected embryos showed a decrease in hindgut expression of a putative *Sp-Pdx1* CRM5-GFP construct that normally shows *Sp-Pdx1*-like expression pattern. This allowed us to validate the cis-regulatory direct effect of Sp-Hox11/13b on *Sp-Pdx1* via *Sp-Pdx1* CRM5 (Figure 7 green diamond). The cis-regulatory effect of Sp-Tcf on *Sp-Hox11/13b* and *Sp-Blimp1* has been shown previously at blastula 18-24 hours post fertilization (Cui et al., 2017; Smith et al., 2008), and our data suggests that these effects persists in the 2 dpf gastrula as well (Figure 7 orange diamonds). In addition, we have also shown that many of the previously identified interactions are indirect and happen via intermediates suggesting high complexity and depth of the 2 dpf sea urchin hindgut GRN even for nodes co-expressed with *Sp-Pdx1* (Figure 7).

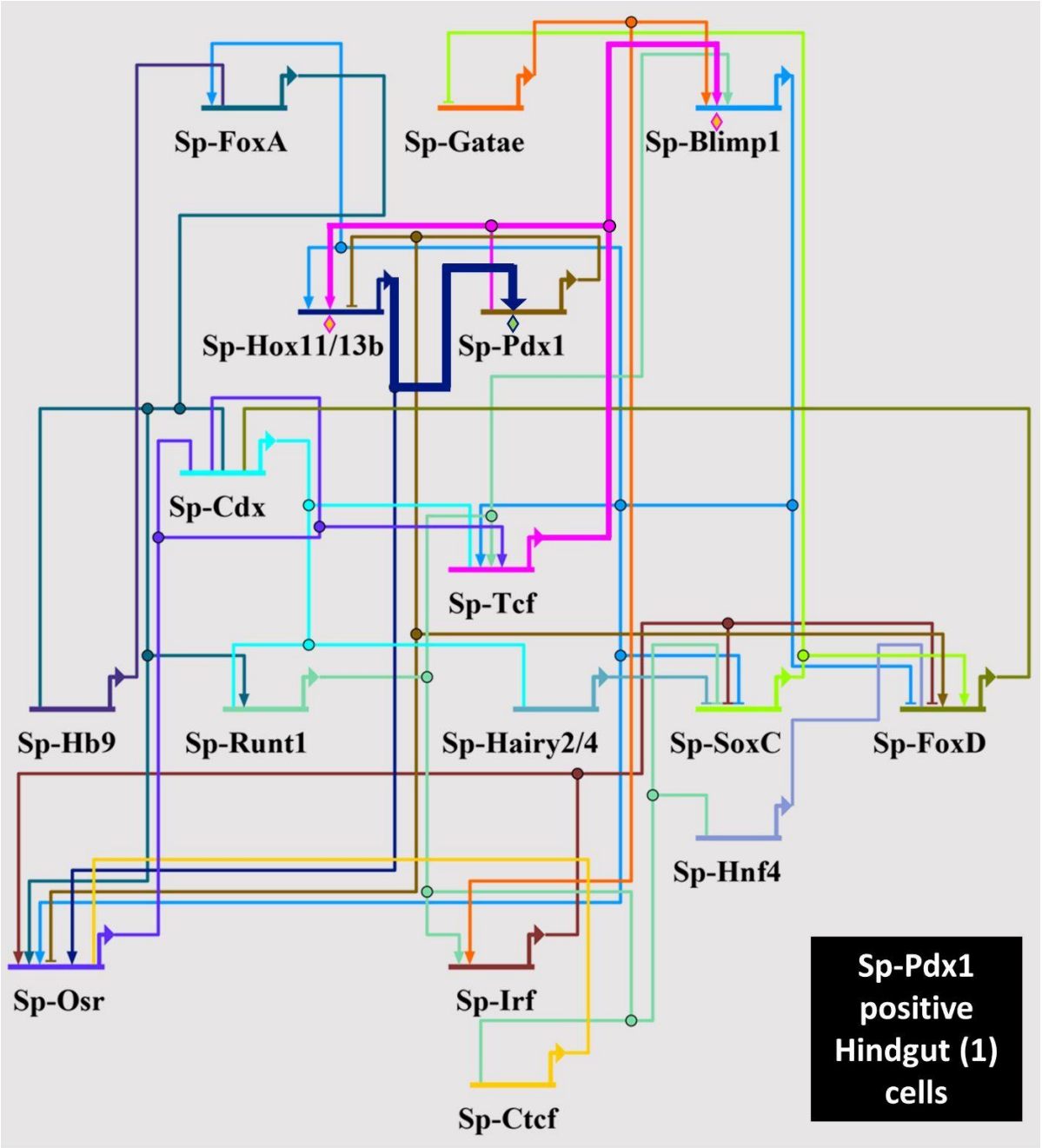

Figure 7. GRN operating in Sp-Pdx1 positive hindgut cells. Updated GRN of previously published nodes within Sp-Pdx1 positive hindgut cells drafted using the presented multi-omics approach.

Discussion

Predicted GRNs recapitulate and refine existing GRN

The sea urchin endomesoderm GRN is one of the most studied GRNs in echinoderm research. However, the GRNs were traditionally drafted for morphologically

identifiable tissues which may or may not express all the nodes at a particular time point. In addition, historically, GRNs had limited information, mostly due to lack of high-throughput technologies at the time, on whether a particular interaction is direct or indirect, unless cis-regulatory analysis was performed. Lack of information as to the directness, allows only the overall final effect of perturbation on a gene to be identified. The integrative multi-omics allows us to solve these issues. The GRN presented in this manuscript is the first GRN for a cell population expressing a particular TF, in this case *Sp-Pdx1*, and all the nodes are shown to be co-expressed with *Sp-Pdx1* in the same cells by scRNA-seq data. ATAC-seq data, on the other hand, points to which interactions of the GRN are likely to be direct and which are not, and through which intermediates they could go. These intermediates allow deducing the most parsimonious effect of a gene perturbation on the downstream targets, direct or indirect. Thus, the available omics data allows to tackle sea urchin GRNs at unprecedented resolution, which refines the existing GRNs and highlights the complexity and depth of the regulatory wiring responsible for the development of cell types, tissues and other embryonic structures. Our data suggests that the hindgut GRN, and likely, the whole endomesoderm GRN, is more complex and diverse with many TF genes serving as intermediates in the interactions of the GRN nodes.

The published interactions of the hindgut GRN were recapitulated through our approach, albeit showing that most of them are likely indirect, increasing the resolution of the interactions of the nodes. The approach stays within the logic of Materna and Oliveri 2008 for drafting GRNs as the embryological knowledge is obtained via scRNA-seq data while the knowledge of the regulatory genes such as TFs as well as CRMs that establish the regulatory state are identified via ATAC-seq and scRNA-seq datasets. Finally, the causal information can be added through differential bulk RNA-seq after gene perturbation. Thus, all the necessary components for GRN drafting as per Materna and Oliveri 2008 can be obtained through this integrative approach.

Limitations and strengths of the approach

This approach has its own limitations. Majority of TF position weight matrices (PWMs) are available for human or mouse TFs (Fornes et al., 2020) only with very

few sea urchin PWM published. Thus, human homologs are used for TF footprinting, which could lead to false negatives or positives if the sea urchin homologs have different binding sequences. In addition, certain TFs have similar PWMs such as forkhead genes (FoxD, FoxA etc) which complicates identification of TFs binding to a particular locus in a CRM.

The tools available are designed for cell cultures, so data from whole tissue/embryo is likely to involve a lot of noise, and some gut interactions could potentially be hidden by reads coming from mesodermal cells still attached at the tip of the archenteron (presumptive coelomic pouches or muscles) that have a different TF repertoire bound to their DNA that could be left over during the gut tissue preparation. This could lead to false positives and false negatives. Thus, the indicative nature of the approach highlights the need for *in vivo* validations. With CRM analysis data lacking for 2 dpf, experimental *in vivo* validations are necessary to validate the results of our approach at this stage of embryo development.

It is also important to note that our approach does not take into account cases in which transcription factors operate within a cell type, while they are not actively transcribed by its cells. Such are the cases of protein remainants from a previous developmental timepoint that could still be active, due to the larger protein half-life. For instance, *Sp-Pdx1* could affect more cells than the ones actively expressing it at 2 dpf gastrula stage as Sp-Pdx1 protein could persist in the cells and continue to function after active transcription and translation of this TF have ended. Thus, more cells of the hindgut could have genes under Sp-Pdx1 control if these cells were expressing *Sp-Pdx1* earlier in development.

Despite the highlighted limitations, the importance of multimodal approaches to improve GRN inference has been recently highlighted (van der Sande et al., 2023). Our approach takes advantage of multi omics datasets that are fairly few for sea urchins but numerous for human and mouse experimental systems (Allen et al., 2023; Burda et al., 2022; Chen et al., 2023; Luo et al., 2022) to improve GRN specificity, depth and directionality. With the high availability of chromatin accessibility data, especially, coupled with chromosome conformation capture to improve predictions of enhancer targets and with scRNA-seq data to identify cell type families and transcript repertoires, such an approach can effectively be applied

to human, mouse or any other species with similar datasets available. Using sea urchins, however, it is also possible to perform validations of the computational predictions *in vivo* on the whole embryo, unlike species where such high throughput validations would have to be confined to cell line cultures. Overall, applying such approaches within echinoderm research has the potential of giving a more holistic view of gene regulation in a specific cell type in a developing embryo.

Materials and Methods

Animal husbandry and culture of embryos

Adult *Strongylocentrotus purpuratus* individuals were obtained from Patrick Leahy (Kerckhoff Marine Laboratory, California Institute of Technology, Pasadena, CA, USA) and maintained in circulating seawater aquaria at Stazione Zoologica Anton Dohrn in Naples. Gametes were obtained by vigorously shaking the animals. Embryos and larvae were cultured at 15 °C in filtered Mediterranean Sea water diluted 9:1 with deionized water and collected 2 days post fertilization (dpf).

Gut tissue separation

Sea urchin gut tissue was obtained by adapting existing protocols (Juliano et al., 2014; McClay, 2004). Echinoderm embryos were grown until the 2 dpf gastrula stage. The embryo suspensions were collected into 1.5 mL tubes using a 40 µm Nitex mesh filter and concentrated by spinning at 500 g for 5 min at 4°C and then washed once in 1 mL of Ca^{2+}-Mg^{2+} free sea water (CMFSW). Then, the embryos were concentrated again by centrifuging at 500 g for 5 min at 4°C and treated with 1M glycine 0.02M EDTA in CMFSW for 10 minutes on ice. Embryos are pipetted up and down carefully using P1000 micropipette three times and transferred onto 1% agarose plates under the dissecting microscope to control the dissociation process. The guts were then collected individually into 1.5 ml Eppendorf tubes with 100 µl of artificial sea water on ice.

ATAC-seq library synthesis

ATAC-seq libraries were generated as described in Magri et al. (2021). Around 270 gastrula stage embryos or 400 embryonic guts were collected per biological replicate

and washed on the 40 µm Nitex mesh filter with artificial sea water (28.3g NaCl, 0.77g KCl, 5.41g $MgCl_2 \cdot 6H_2O$, 3.42g $MgSO_4$ or 7.13g $MgSO_4 \cdot 7H_2O$, 0.2g $NaHCO_3$, 1.56g $CaCl_2 \cdot 2H_2O$ per 1 L of deionized water) and transferred into 1.5 ml tubes. The samples were then centrifuged at 500 g for 5 min at 4 °C, washed twice with 200 µl artificial sea water in the 1.5 ml tube and then resuspended in 50 µl of lysis buffer (10 mM Tris-HCl, pH 7.4, 10 mM NaCl, 3 mM MgCl2, 0.2% IGEPAL CA-630), followed by lysis by pipetting up and down for 3-5 minutes. Half of the lysate was used for counting the released nuclei under Zeiss AxioImager M1 microscope using a haemocytometer with DAPI dye (1µl of 1:100 diluted DAPI in the 25 µl of the released nuclei). The other half was used for the tagmentation reaction by centrifuging the sample at 500 g, removing lysis buffer and then incubating for 30 minutes at 37°C with 25 µl of 2x tagmentation buffer (20 mM Tris-HCl, 10 mM MgCl2, 20% (vol/vol) dimethylformamide), 23.75 µl of nuclease free water and 1.25 µl of Tn5 enzyme. The Tn5 enzyme used for ATAC-seq library preparations was provided by Dr Jose Luis Gómez-Skarmeta.

The tagmented DNA was purified using MinElute Kit (Qiagen) following manufacturer's instructions and eluted in 10µl of elution buffer. The eluted DNA was then amplified to obtain the library for sequencing (10 µl of eluted tagmented DNA, 10 µl of nuclease free water, 2.5 µl 10 µM Nextera Primer 1, 2.5 µl 10 µM Nextera Primer 2.X, where X is the unique Nextera barcode used for sequencing and 25 µl of NEBNext High-Fidelity 2x PCR Master Mix (New England BioLabs) using the following thermocycler program: 72°C for 5 min, 98°C for 30 sec, then 15 cycles of 98 °C for 10 sec, 63 °C for 30 sec and 72 °C for 1 min, followed by a hold step at 4°C. The amplified library was then purified with MinElute Kit (Qiagen) following manufacturer's instructions and eluted in 20 µl of elution buffer. The concentration of the resulting library was checked using Qubit dsDNA BR Assay Kit (Molecular Probes) and its quality was assessed by running 70 µg of the library on 2% agarose 1x TAE gel. Libraries exhibiting nucleosomal size patterns on the gel were sent for sequencing. Sequencing was performed by BGI Tech (HongKong) resulting in 50 bp paired-end reads (Illumina HiSeq 4000) with mean of 57 M reads.

ATAC-seq data analysis

The raw ATAC-seq reads were trimmed from adapter sequences and bad quality bases using Trimmomatic 0.38 (Bolger et al., 2014) using the following parameters ILLUMINACLIP:TruSeq3-PE-2.fa:2:30:10:6 CROP:40 SLIDINGWINDOW:3:25 MINLEN:25 for paired end data and -phred33 quality scores. The good quality reads from each replicate are then mapped to the *S. purpuratus* genome v3.1 (Sea Urchin Genome Sequencing Consortium et al., 2006) using bowtie2 2.3.4.1 (Langmead and Salzberg, 2012). The mapped reads in BAM format were then converted into bed files using bedtools 2.27.1 (Quinlan and Hall, 2010), the bam file was filtered using samtools 1.7.1 (Li et al., 2009) to keep aligned reads of quality greater than 30, fix mates and remove duplicates with default parameters. In addition, only fragments of less than 130 bp in size were kept. The resulting files were then used in MACS2 2.1.2 software (Zhang et al., 2008) to call peaks using BED as input file format as well as setting --extsize to 100, --shift to 50 and using --nomodel setting with genome size of 815936258 for *S. purpuratus* genome v3.1; all the other MACS2 settings were kept at default. Bedtools 2.26.0 intersect tool (Quinlan and Hall, 2010) was used with default settings to combine replicates and obtain a set of concordant peaks, which were then all merged using bedtools merge to putative cis-regulatory modules (pCRMs) list.

The resulting gut ATAC-seq bam files were merged using bamtools and used as input in TOBIAS 0.11.1-dev (Bentsen et al., 2020) along with the genome and CRM list to perform transcription factor (TF) footprinting analysis. TOBIAS commands ATACorrect and ScoreBigwig were run with default parameters, BINDetect was run using JASPAR2020 vertebrate motif database position weight matrices (PWMs) (Fornes et al., 2020) using --motif-pvalue of 1e-5. Motifs for each TF with score of at least 0.5 were kept, to obtain a table with each pCRM and TFs bound to it. HOMER 4.10.3 (Heinz et al., 2010) annotatePeaks.pl was used to assign pCRMs to *S. purpuratus* genes. BLAST 2.6.0+ (Altschul et al., 1990) with max_target_seqs of 1 and max_hsps of 1 was used to identify single best sea urchin homolog for each of vertebrate TFs.

Single cell embryo dissociation

Dissociation of the 2 dpf *Strongylocentrotus purpuratus* gastrulae into single cells was performed the same as in Paganos et al. (2021). Embryos were collected, concentrated using a 40 µm Nitex mesh filter and spun down at 500 g for 10 min. Sea water was removed and larvae were resuspended in $Ca^{2+}Mg^{2+}$-free artificial sea water. Embryos were concentrated at 500 g for 10 min at 4 °C and resuspended in a dissociation buffer containing 1 M glycine and 0.02 M EDTA in $Ca^{2+}Mg^{2+}$-free artificial sea water. Embryos were incubated on ice for 10 min and mixed gently approximately every 2 min, monitoring the progress of the dissociation. Dissociated cells were concentrated at the bottom of the tube at 700 g for 5 min and washed several times with $Ca^{2+}Mg^{2+}$-free artificial sea water. Cell viability was assessed using propidium iodide and fluorescein diacetate, samples with cell viability ≥ 90 % were further processed. Single cells were counted using a hemocytometer and diluted according to the manufacturer's protocol (10X Genomics).

Single-cell RNA sequencing and data analysis

ScRNA-seq sequencing and the analysis of the 2 dpf *Strongylocentrotus purpuratus* gastrula stage data was performed the same as in Paganos et al. (2021). Single cell RNA sequencing was performed using the 10X Genomics single-cell capturing system. Cells from three biological replicates, ranging from 6000 to 20,000 cells, were loaded on the 10X Genomics Chromium Controller. Single cell cDNA libraries were prepared using the Chromium Single Cell 3' Reagent Kit (v3 and v3.1). Libraries were sequenced by GeneCore (EMBL, Heidelberg, Germany) for 75 bp paired-end reads (Illumina NextSeq 500). Cell Ranger Software Suite 3.0.2 (10x Genomics) was used for the alignment of the single-cell RNA-seq output reads and generation of feature, barcode and matrices. The genomic index was made in Cell Ranger using the *S. purpuratus* genome version 3.1 (Kudtarkar and Cameron, 2017; Sea Urchin Genome Sequencing Consortium et al., 2006). Cell Ranger output matrices for three biological and two technical replicates were used for further analysis in Seurat v3.0.2 R package (Stuart et al., 2019). Genes that are transcribed in less than three cells and cells that have less than a minimum of 200 transcribed genes were excluded from the analysis. The cutoff number of transcribed genes was determined based on feature scatter plots and varies depending on the replicate. In

total 15,341 cells passed the quality checks and were further analyzed. Datasets were normalized and variable genes were found using the vst method with a maximum of 2000 variable features. Data integration was performed via identification of anchors between the five different objects. Next the datasets were scaled and principal component (PCA) analysis was performed. Nearest Neighbor (SNN) graph was computed with 20 dimensions (resolution 1.0) to identify the clusters. Transcripts of all genes per cell type were identified by converting a Seurat DotPlot with all these transcripts as features into a table (ggplot2 3.2.0 R package). All resulting tables containing the genes transcribed within different cell type families were further annotated adding PFAM terms (Finn et al., 2014; Trapnell et al., 2010) for associated proteins, gene ontology terms and descriptions from Echinobase (Kudtarkar and Cameron, 2017).

Morpholino injections

Microinjections were performed as follows. The sea urchin eggs were dejellied in acidic seawater (pH 4.5) for <1 min, then washed in filtered sea water and rowed onto 4% protamine sulfate plates filled with PABA-FSW (50 mg of p-aminobenzoic acid in 100 ml of filtered sea water). The microinjecting needle was pulled from borosilicate glass with capillary using Sutter Instrument Co. Novato, CA using P-97 micropipette puller (Sutter), was loaded with the injection solution using a Microloader pipette tip (Eppendorf). Loaded needle tip was broken off using a scratch in the middle of the protamine plate with eggs. The eggs were fertilized with a few drops of diluted sea urchin sperm and injected with approximately 2 pL of microinjection solution. Injected eggs were washed twice with filtered sea water and incubated at 15 °C overnight, then the hatched embryos were transferred to 4-well plates (ThermoFisher Scientific) with filtered sea water to grow until 2 days post fertilization gastrula stage.

The morpholino oligonucleotide (MO) microinjection solutions containing contained 100 μM of final morpholino concentration were heated up to 75°C for 5 min and then passed through a 0.22 μm PVDF micro-filter (Millipore) placed in 500 μl tube by centrifugation at 2500 g for 2 min. After filtration, the filtrate was centrifuged for 15 min at top speed prior to microinjection. The translation morpholino sequence for *Sp-Hox11/13b* is the same as previously described (Arenas-Mena et al., 2006).

RNA-seq data analysis

Raw reads for 2 dpf *Sp-Pdx1* MO injected and untreated embryos were published in Annunziata and Arnone (2014). The reads were re-analyzed for this manuscript, adhering to more up to date pipelines. Fastqc 0.11.5 (Andrews, 2010) was used to assess the quality of sequencing data. Bad quality sequences were trimmed from the reads using Trimmomatic 0.38 (Bolger et al., 2014) with the following options ILLUMINACLIP:TruSeq3-PE-2.fa:2:30:10:6 CROP:90 HEADCROP:10 SLIDINGWINDOW:3:25 MINLEN:25 using -phred33 base quality encoding for paired end reads. Only the paired output of Trimmomatic was used as input in Salmon 0.11.3 (Patro et al., 2017) for transcript quantification with automatic library detection and all settings left as default. Salmon index was made using transcriptome FASTA file corresponding with *S. purpuratus* genome version 3.1 from Echinobase.org (Cary et al., 2018; Tu et al., 2012) with k value of 25. The Salmon output quants files were used in DESeq2 (Love et al., 2014) R package for differential gene expression analysis; tximport (Soneson et al., 2015) package was used to link every transcript to a WHL ID denoting genes in the genome annotation. The analysis was performed using local fit and ~condition (untreated or MO injected) as the factor. Differentially expressed transcripts with p-adjusted value of less than 0.05 using independent hypothesis weighting (IHW) were considered significant. Resulting transcripts were annotated adding *S. purpuratus* gene names.

***In silico* GRN drafting**

The table with each putative sea urchin CRM and TFs bound to it, along with their target genes (described in ATAC-seq data analysis) was filtered to have only TFs and target genes present in a single cell type family. For this, the tables containing the genes transcribed within different cell type families, obtained in scRNA-seq data analysis as described above, were cut to have only genes expressed in the hindgut cluster. This list was used for filtering of the ATAC-seq analysis results. The resulting table of TFs and target genes was further filtered to have only TFs (Lambert et al., 2018) both as target and effector. In order to build a network downstream of Sp-Pdx, the data was further narrowed down to contain only genes expressed in *Sp-Pdx* positive cells. For this, AddModuleScore from Seurat (Stuart et al., 2019) was used to assess expression of *Sp-Pdx1* in the 2 dpf cells; only cells where the resulting

value was greater than 1.5 belonging to the hindgut cells cluster were taken for further analysis. Genes expressed in those cells with scaled average expression greater than 0.5 were used to build the GRN downstream of Sp-Pdx1 positive cells. To predict causal information of the interactions within the Sp-Pdx1 network results of the bulk RNA-seq differential expression analyses between untreated embryos and Sp-Pdx1 morpholino injected embryos were used. With the help of a custom R 4.1.2 (R Core Team, 2021) script direct targets of Sp-Pdx1 (based on ATAC-seq data) within *Sp-Pdx1* positive cells were assigned causal dynamics information, then the targets of the direct targets, then the targets of indirect targets. This process was performed iteratively to give most parsimonious causal information to the genes downstream of Sp-Pdx1 in the GRN.

CRM GFP reporter construct synthesis

Tagging of putative CRMs was performed according to a protocol described by Nam et al. (2010). The plasmids with DNA tags were provided by Dr Jongmin Nam. 50 bp flanks from the genome were added to the pCRMs to design primers using Primer3web 4.1.0 (Untergasser et al., 2012) falling within the added 50 bp to ensure the whole CRM is amplified. 18bp of the reverse complement of the beginning of the DNA tag sequences was added to the 5’ of the reverse primer so that the CRM can be combined with the DNA tag in equal amount using overlap PCR (Xiong et al., 2006) using Expand High Fidelity PLUS PCR (Sigma). The resulting fragment was run on 2% agarose 1x TAE gel, the corresponding band was cut out, and gel purified using GenElute Gel Extraction Kit (Sigma) according to manufacturer's guidelines and eluted in 50 µl of kit elution buffer. The eluted DNA was then purified again using QIAquick PCR Purification Kit (Qiagen) and eluted in 30 µl of kit elution buffer. DNA yield and concentration was assessed using NanoDrop ND-1000 (ThermoFisher Scientific).

CRM GFP reporter construct injections

The tagged CRM was used to make microinjection solutions according to Nam et al. (2010): 0.5 µl of tagged CRM solution, 1.2 µl of 1 mM KCl, 0.275 µl carrier DNA (genomic DNA sheared with HindIII enzyme (2 units for µg of DNA, in SuRE/Cut Buffer B for 3 h at 37 °C), purified using QIAquick PCR Purification Kit (Qiagen) and diluted to 500 ng/µl) and water up to 10 µl (Arnone et al., 2004; Nam et al., 2010).

The prepared solutions were then centrifuged at top speed for 15 min until microinjections. The microinjection procedure was the same as described in Morpholino injections.

Fluorescent *in situ* hybridization (FISH)

FISH was performed as described in Paganos et al. (2022a). In brief, embryos were collected 2 dpf and fixed in 4% PFA in MOPS Buffer overnight at 4°C. The following day specimens were washed with MOPS buffer several times and then stored in 70% ethanol at −20°C. Antisense mRNA probes were generated as described in Perillo et al. (2021). The primer sequences used for cDNA isolation were the same as previously described: *Sp-Synb (Burke et al., 2006)*, *Sp-FoxA*, *Sp-Pdx1, Sp-Brn1/2/4, Sp-Cdx, Sp-ManrC1a, Sp-Hox11/13b* (Annunziata and Arnone, 2014); *Sp-FoxC* (Andrikou et al., 2015); *Sp-Ptf1a* (Perillo et al., 2016); *Sp-Pks1 (Perillo et al., 2020)*; SPU_006199, Sp-Fbsl_2, S*p-Bra, Sp-FoxABL, Sp-Frizz5/8* and *Sp-FcoII/II/III, Sp-Hypp_1249, Sp-Mlckb, Sp-Hypp_2386* (Paganos et al., 2021). Probes were synthesized from linearized DNA and labeled during synthesis with digoxigenin-11-UTP (Roche) nucleotides. Fluorescent signal was developed using the fluorophore conjugated tyramide technology. Specimens were imaged using a Zeiss LSM 700 confocal microscope.

References

Allen WE, Blosser TR, Sullivan ZA, Dulac C, Zhuang X. 2023. Molecular and spatial signatures of mouse brain aging at single-cell resolution. *Cell* **186**:194–208.e18.

Altschul SF, Gish W, Miller W, Myers EW, Lipman DJ. 1990. Basic local alignment search tool. *J Mol Biol* **215**:403–410.

Amore G, Yavrouian RG, Peterson KJ, Ransick A, McClay DR, Davidson EH. 2003. Spdeadringer, a sea urchin embryo gene required separately in skeletogenic and oral ectoderm gene regulatory networks. *Dev Biol* **261**:55–81.

Andrews S. 2010. FastQC: a quality control tool for high throughput sequence data.

Andrikou C, Iovene E, Rizzo F, Oliveri P, Arnone MI. 2013. Myogenesis in the sea urchin embryo : the molecular fingerprint of the myoblast precursors Myogenesis in the sea urchin embryo : the molecular fingerprint of the myoblast precursors. *Evodevo*. doi:10.1186/2041-9139-4-33

Andrikou C, Pai C-Y, Su Y-H, Arnone MI. 2015. Logics and properties of a genetic regulatory program that drives embryonic muscle development in an echinoderm. *Elife* **4**. doi:10.7554/eLife.07343

Annunziata R, Andrikou C, Perillo M, Cuomo C, Arnone MI. 2019. Development and evolution of gut structures: from molecules to function. *Cell Tissue Res*

377:445–458.
Annunziata R, Arnone MI. 2014. A dynamic regulatory network explains ParaHox gene control of gut patterning in the sea urchin. *Development* **141**:2462–2472.
Arenas-Mena C, Cameron RA, Davidson EH. 2006. Hindgut specification and cell-adhesion functions of Sphox11/13b in the endoderm of the sea urchin embryo. *Dev Growth Differ* **48**:463–472.
Arnone MI, Byrne M, Martinez P. 2015. Echinodermata. *Evolutionary Developmental Biology of Invertebrates 6* 1–58.
Arnone MI, Dmochowski IJ, Gache C. 2004. Using reporter genes to study cis-regulatory elements. *Methods Cell Biol* **74**:621–652.
Arnone MI, Martin EL, Davidson EH. 1998. Cis-regulation downstream of cell type specification: a single compact element controls the complex expression of the CyIIa gene in sea urchin embryos. *Development* **125**:1381–1395.
Bentsen M, Goymann P, Schultheis H, Klee K, Petrova A, Wiegandt R, Fust A, Preussner J, Kuenne C, Braun T, Kim J, Looso M. 2020. ATAC-seq footprinting unravels kinetics of transcription factor binding during zygotic genome activation. *Nat Commun* **11**:4267.
Bolger AM, Lohse M, Usadel B. 2014. Trimmomatic: a flexible trimmer for Illumina sequence data. *Bioinformatics* **30**:2114–2120.
Buenrostro JD, Wu B, Chang HY, Greenleaf WJ. 2015. ATAC-seq: A Method for Assaying Chromatin Accessibility Genome-WideCurrent Protocols in Molecular Biology. Hoboken, NJ, USA: John Wiley & Sons, Inc. pp. 21.29.1–21.29.9.
Burda JE, O'Shea TM, Ao Y, Suresh KB, Wang S, Bernstein AM, Chandra A, Deverasetty S, Kawaguchi R, Kim JH, McCallum S, Rogers A, Wahane S, Sofroniew MV. 2022. Divergent transcriptional regulation of astrocyte reactivity across disorders. *Nature* **606**:557–564.
Burke RD, Osborne L, Wang D, Murabe N, Yaguchi S, Nakajima Y. 2006. Neuron-specific expression of a synaptotagmin gene in the sea urchin Strongylocentrotus purpuratus. *J Comp Neurol* **496**:244–251.
Cary GA, Cameron RA, Hinman VF. 2018. EchinoBase: Tools for Echinoderm Genome Analyses. *Methods Mol Biol* **1757**:349–369.
Cary GA, McCauley BS, Zueva O, Pattinato J, Longabaugh W, Hinman VF. 2020. Systematic comparison of sea urchin and sea star developmental gene regulatory networks explains how novelty is incorporated in early development. *Nat Commun* **11**:6235.
Chen W-J, Dong K-Q, Pan X-W, Gan S-S, Xu D, Chen J-X, Chen W-J, Li W-Y, Wang Y-Q, Zhou W, Rini B, Cui X-G. 2023. Single-cell RNA-seq integrated with multi-omics reveals SERPINE2 as a target for metastasis in advanced renal cell carcinoma. *Cell Death Dis* **14**:30.
Cole AG, Arnone MI. 2009. Fluorescent in situ hybridization reveals multiple expression domains for SpBrn1/2/4 and identifies a unique ectodermal cell type that co-expresses the ParaHox gene SpLox. *Gene Expr Patterns* **9**:324–328.
Cole AG, Rizzo F, Martinez P, Fernandez-Serra M, Arnone MI. 2009. Two ParaHox genes, SpLox and SpCdx, interact to partition the posterior endoderm in the formation of a functional gut. *Development* **136**:541–549.
Cui M, Siriwon N, Li E, Davidson EH, Peter IS. 2014. Specific functions of the Wnt signaling system in gene regulatory networks throughout the early sea urchin embryo. *Proc Natl Acad Sci U S A* **111**:E5029–38.
Cui M, Vielmas E, Davidson EH, Peter IS. 2017. Sequential Response to Multiple Developmental Network Circuits Encoded in an Intronic cis- Regulatory Module

of Sea Urchin hox11/13b. *Cell Rep* **19**:364–374.
Davidson PL, Guo H, Swart JS, Massri AJ, Edgar A, Wang L, Berrio A, Devens HR, Koop D, Cisternas P, Zhang H, Zhang Y, Byrne M, Fan G, Wray GA. 2022. Recent reconfiguration of an ancient developmental gene regulatory network in Heliocidaris sea urchins. *Nat Ecol Evol* **6**:1907–1920.
de-Leon SB-T, Davidson EH. 2010. Information processing at the foxa node of the sea urchin endomesoderm specification network. *Proceedings of the National Academy of Sciences* **107**:10103–10108.
Ettensohn CA. 2020. The gene regulatory control of sea urchin gastrulation. *Mech Dev* **162**:103599.
Finn RD, Bateman A, Clements J, Coggill P, Eberhardt RY, Eddy SR, Heger A, Hetherington K, Holm L, Mistry J, Sonnhammer ELL, Tate J, Punta M. 2014. Pfam: the protein families database. *Nucleic Acids Res* **42**:D222–D230.
Fornes O, Castro-Mondragon JA, Khan A, van der Lee R, Zhang X, Richmond PA, Modi BP, Correard S, Gheorghe M, Baranašić D, Santana-Garcia W, Tan G, Chèneby J, Ballester B, Parcy F, Sandelin A, Lenhard B, Wasserman WW, Mathelier A. 2020. JASPAR 2020: update of the open-access database of transcription factor binding profiles. *Nucleic Acids Res* **48**:D87–D92.
Harkey MA, Whiteley HR, Whiteley AH. 1992. Differential expression of the msp130 gene among skeletal lineage cells in the sea urchin embryo: a three dimensional in situ hybridization analysis. *Mech Dev* **37**:173–184.
Heinz S, Benner C, Spann N, Bertolino E, Lin YC, Laslo P, Cheng JX, Murre C, Singh H, Glass CK. 2010. Simple combinations of lineage-determining transcription factors prime cis-regulatory elements required for macrophage and B cell identities. *Mol Cell* **38**:576–589.
Ho EC, Buckley KM, Schrankel CS, Schuh NW, Hibino T, Solek CM, Bae K, Wang G, Rast JP. 2017. Perturbation of gut bacteria induces a coordinated cellular immune response in the purple sea urchin larva. *Immunol Cell Biol* **95**:647.
Juliano CE, Yajima M, Wessel GM. 2010. Nanos functions to maintain the fate of the small micromere lineage in the sea urchin embryo. *Dev Biol* **337**:220–232.
Juliano C, Swartz SZ, Wessel G. 2014. Isolating specific embryonic cells of the sea urchin by FACS. *Methods Mol Biol* **1128**:187–196.
Kudtarkar P, Cameron RA. 2017. Echinobase: an expanding resource for echinoderm genomic information. *Database* **2017**. doi:10.1093/database/bax074
Lambert SA, Jolma A, Campitelli LF, Das PK, Yin Y, Albu M, Chen X, Taipale J, Hughes TR, Weirauch MT. 2018. The Human Transcription Factors. *Cell* **175**:598–599.
Langmead B, Salzberg SL. 2012. Fast gapped-read alignment with Bowtie 2. *Nat Methods* **9**:357–359.
Lee PY, Nam J, Davidson EH. 2007. Exclusive developmental functions of gatae cis-regulatory modules in the Strongylocentrorus purpuratus embryo. *Dev Biol* **307**:434–445.
Li H, Handsaker B, Wysoker A, Fennell T, Ruan J, Homer N, Marth G, Abecasis G, Durbin R, 1000 Genome Project Data Processing Subgroup. 2009. The Sequence Alignment/Map format and SAMtools. *Bioinformatics* **25**:2078–2079.
Livi CB, Davidson EH. 2007. Regulation of spblimp1/krox1a, an alternatively transcribed isoform expressed in midgut and hindgut of the sea urchin gastrula. *Gene Expr Patterns* **7**:1–7.
Love MI, Huber W, Anders S. 2014. Moderated estimation of fold change and

dispersion for RNA-seq data with DESeq2. *Genome Biol* **15**:550.
Lowe EK, Cuomo C, Arnone MI. 2016. A Differential Transcriptomic Approach to Compare Target Genes of Homologous Transcription Factors in Echinoderm Species. Cham: Springer International Publishing.
Luo L, Gribskov M, Wang S. 2022. Bibliometric review of ATAC-Seq and its application in gene expression. *Brief Bioinform* **23**. doi:10.1093/bib/bbac061
Magri MS, Voronov D, Ranđelović J, Cuomo C, Gómez-Skarmeta JL, Arnone MI. 2021. ATAC-Seq for Assaying Chromatin Accessibility Protocol Using Echinoderm Embryos. *Methods Mol Biol* **2219**:253–265.
Massri AJ, Greenstreet L, Afanassiev A, Berrio A, Wray GA, Schiebinger G, McClay DR. 2021. Developmental single-cell transcriptomics in the Lytechinus variegatus sea urchin embryo. *Development* **148**. doi:10.1242/dev.198614
Materna SC, Oliveri P. 2008. A protocol for unraveling gene regulatory networks. *Nat Protoc* **3**:1876–1887.
McCarty CM, Coffman JA. 2013. Developmental cis-regulatory analysis of the cyclin D gene in the sea urchin Strongylocentrotus purpuratus. *Biochem Biophys Res Commun* **440**:413–418.
McClay DR. 2011. Evolutionary crossroads in developmental biology: sea urchins. *Development* **138**:2639–2648.
McClay DR. 2004. Methods for embryo dissociation and analysis of cell adhesion. *Methods Cell Biol* **74**:311–329.
Nam J, Dong P, Tarpine R, Istrail S, Davidson EH. 2010. Functional cis-regulatory genomics for systems biology. *Proceedings of the National Academy of Sciences*. doi:10.1073/pnas.1000147107
Paganos P, Caccavale F, La Vecchia C, D'Aniello E, D'Aniello S, Arnone MI. 2022a. FISH for All: A Fast and Efficient Fluorescent In situ Hybridization (FISH) Protocol for Marine Embryos and Larvae. *Front Physiol* **13**. doi:10.3389/fphys.2022.878062
Paganos P, Ronchi P, Carl J, Mizzon G, Martinez P, Benvenuto G, Arnone MI. 2022b. Integrating single cell transcriptomics and volume electron microscopy confirms the presence of pancreatic acinar-like cells in sea urchins. *Front Cell Dev Biol* **10**:991664.
Paganos P, Ullrich-Lüter E, Caccavale F, Zakrzewski A, Voronov D, Fournon-Berodia I, Cocurullo M, Lüter C, Arnone MI. 2022c. A New Model Organism to Investigate Extraocular Photoreception: Opsin and Retinal Gene Expression in the Sea Urchin. *Cells* **11**. doi:10.3390/cells11172636
Paganos P, Voronov D, Musser JM, Arendt D, Arnone MI. 2021. Single-cell RNA sequencing of the larva reveals the blueprint of major cell types and nervous system of a non-chordate deuterostome. *Elife* **10**. doi:10.7554/eLife.70416
Patro R, Duggal G, Love MI, Irizarry RA, Kingsford C. 2017. Salmon provides fast and bias-aware quantification of transcript expression. *Nat Methods* **14**:417–419.
Perillo M, Oulhen N, Foster S, Spurrell M, Calestani C, Wessel G. 2020. Regulation of dynamic pigment cell states at single-cell resolution. *Elife* **9**. doi:10.7554/eLife.60388
Perillo M, Paganos P, Spurrell M, Arnone MI, Wessel GM. 2021. Methodology for Whole Mount and Fluorescent RNA In Situ Hybridization in Echinoderms: Single, Double, and Beyond. *Methods Mol Biol* **2219**:195–216.
Perillo M, Wang YJ, Leach SD, Arnone MI. 2016. A pancreatic exocrine-like cell regulatory circuit operating in the upper stomach of the sea urchin

Strongylocentrotus purpuratus larva. *BMC Evol Biol* **16**:117.
Peter IS, Davidson EH. 2010. The endoderm gene regulatory network in sea urchin embryos up to mid-blastula stage. *Dev Biol* **340**:188–199.
Poustka AJ, Kühn A, Radosavljevic V, Wellenreuther R, Lehrach H, Panopoulou G. 2004. On the origin of the chordate central nervous system: expression of onecut in the sea urchin embryo. *Evol Dev* **6**:227–236.
Quinlan AR, Hall IM. 2010. BEDTools: a flexible suite of utilities for comparing genomic features. *Bioinformatics* **26**:841–842.
Rafiq K, Shashikant T, McManus CJ, Ettensohn CA. 2014. Genome-wide analysis of the skeletogenic gene regulatory network of sea urchins. *Development* **141**:950–961.
R Core Team. 2021. R: A Language and Environment for Statistical Computing.
Röttinger E, Lowe CJ. 2012. Evolutionary crossroads in developmental biology: hemichordates. *Development* **139**:2463–2475.
Schwaiger M, Andrikou C, Dnyansagar R, Murguia PF, Paganos P, Voronov D, Zimmermann B, Lebedeva T, Schmidt HA, Genikhovich G, Benvenuto G, Arnone MI, Technau U. 2022. An ancestral Wnt-Brachyury feedback loop in axial patterning and recruitment of mesoderm-determining target genes. *Nat Ecol Evol* **6**:1921–1939.
Sea Urchin Genome Sequencing Consortium, Sodergren E, Weinstock GM, Davidson EH, Cameron RA, Gibbs RA, Angerer RC, Angerer LM, Arnone MI, Burgess DR, Burke RD, Coffman JA, Dean M, Elphick MR, Ettensohn CA, Foltz KR, Hamdoun A, Hynes RO, Klein WH, Marzluff W, McClay DR, Morris RL, Mushegian A, Rast JP, Smith LC, Thorndyke MC, Vacquier VD, Wessel GM, Wray G, Zhang L, Elsik CG, Ermolaeva O, Hlavina W, Hofmann G, Kitts P, Landrum MJ, Mackey AJ, Maglott D, Panopoulou G, Poustka AJ, Pruitt K, Sapojnikov V, Song X, Souvorov A, Solovyev V, Wei Z, Whittaker CA, Worley K, Durbin KJ, Shen Y, Fedrigo O, Garfield D, Haygood R, Primus A, Satija R, Severson T, Gonzalez-Garay ML, Jackson AR, Milosavljevic A, Tong M, Killian CE, Livingston BT, Wilt FH, Adams N, Bellé R, Carbonneau S, Cheung R, Cormier P, Cosson B, Croce J, Fernandez-Guerra A, Genevière A-M, Goel M, Kelkar H, Morales J, Mulner-Lorillon O, Robertson AJ, Goldstone JV, Cole B, Epel D, Gold B, Hahn ME, Howard-Ashby M, Scally M, Stegeman JJ, Allgood EL, Cool J, Judkins KM, McCafferty SS, Musante AM, Obar RA, Rawson AP, Rossetti BJ, Gibbons IR, Hoffman MP, Leone A, Istrail S, Materna SC, Samanta MP, Stolc V, Tongprasit W, Tu Q, Bergeron K-F, Brandhorst BP, Whittle J, Berney K, Bottjer DJ, Calestani C, Peterson K, Chow E, Yuan QA, Elhaik E, Graur D, Reese JT, Bosdet I, Heesun S, Marra MA, Schein J, Anderson MK, Brockton V, Buckley KM, Cohen AH, Fugmann SD, Hibino T, Loza-Coll M, Majeske AJ, Messier C, Nair SV, Pancer Z, Terwilliger DP, Agca C, Arboleda E, Chen N, Churcher AM, Hallböök F, Humphrey GW, Idris MM, Kiyama T, Liang S, Mellott D, Mu X, Murray G, Olinski RP, Raible F, Rowe M, Taylor JS, Tessmar-Raible K, Wang D, Wilson KH, Yaguchi S, Gaasterland T, Galindo BE, Gunaratne HJ, Juliano C, Kinukawa M, Moy GW, Neill AT, Nomura M, Raisch M, Reade A, Roux MM, Song JL, Su Y-H, Townley IK, Voronina E, Wong JL, Amore G, Branno M, Brown ER, Cavalieri V, Duboc V, Duloquin L, Flytzanis C, Gache C, Lapraz F, Lepage T, Locascio A, Martinez P, Matassi G, Matranga V, Range R, Rizzo F, Röttinger E, Beane W, Bradham C, Byrum C, Glenn T, Hussain S, Manning G, Miranda E, Thomason R, Walton K, Wikramanayke A, Wu S-Y, Xu R, Brown CT, Chen L, Gray RF, Lee PY, Nam J, Oliveri P, Smith J, Muzny D, Bell

S, Chacko J, Cree A, Curry S, Davis C, Dinh H, Dugan-Rocha S, Fowler J, Gill R, Hamilton C, Hernandez J, Hines S, Hume J, Jackson L, Jolivet A, Kovar C, Lee S, Lewis L, Miner G, Morgan M, Nazareth LV, Okwuonu G, Parker D, Pu L-L, Thorn R, Wright R. 2006. The genome of the sea urchin Strongylocentrotus purpuratus. *Science* **314**:941–952.

Shashikant T, Khor JM, Ettensohn CA. 2018. Global analysis of primary mesenchyme cell cis-regulatory modules by chromatin accessibility profiling 1–18.

Smith J, Kraemer E, Liu H, Theodoris C, Davidson E. 2008. A spatially dynamic cohort of regulatory genes in the endomesodermal gene network of the sea urchin embryo. *Dev Biol* **313**:863–875.

Soneson C, Love MI, Robinson MD. 2015. Differential analyses for RNA-seq: transcript-level estimates improve gene-level inferences. *F1000Res* **4**:1521.

Stuart T, Butler A, Hoffman P, Hafemeister C, Papalexi E, Mauck WM 3rd, Hao Y, Stoeckius M, Smibert P, Satija R. 2019. Comprehensive Integration of Single-Cell Data. *Cell* **177**:1888–1902.e21.

Trapnell C, Williams BA, Pertea G, Mortazavi A, Kwan G, van Baren MJ, Salzberg SL, Wold BJ, Pachter L. 2010. Transcript assembly and quantification by RNA-Seq reveals unannotated transcripts and isoform switching during cell differentiation. *Nat Biotechnol* **28**:511–515.

Tu Q, Brown CT, Davidson EH, Oliveri P. 2006. Sea urchin Forkhead gene family: phylogeny and embryonic expression. *Dev Biol* **300**:49–62.

Tu Q, Cameron RA, Worley KC, Gibbs RA, Davidson EH. 2012. Gene structure in the sea urchin Strongylocentrotus purpuratus based on transcriptome analysis. *Genome Res* **22**:2079–2087.

Untergasser A, Cutcutache I, Koressaar T, Ye J, Faircloth BC, Remm M, Rozen SG. 2012. Primer3--new capabilities and interfaces. *Nucleic Acids Res* **40**:e115.

van der Sande M, Frölich S, van Heeringen SJ. 2023. Computational approaches to understand transcription regulation in development. *Biochem Soc Trans* **51**:1–12.

Wei Z, Range R, Angerer R, Angerer L. 2012. Axial patterning interactions in the sea urchin embryo: suppression of nodal by Wnt1 signaling. *Development* **139**:1662–1669.

Xiong A-S, Yao Q-H, Peng R-H, Duan H, Li X, Fan H-Q, Cheng Z-M, Li Y. 2006. PCR-based accurate synthesis of long DNA sequences. *Nat Protoc* **1**:791–797.

Zhang Y, Liu T, Meyer CA, Eeckhoute J, Johnson DS, Bernstein BE, Nusbaum C, Myers RM, Brown M, Li W, Liu XS. 2008. Model-based analysis of ChIP-Seq (MACS). *Genome Biol* **9**:R137.